

# Heat transfer and fluid flow analysis using nanofluids in diamond-shaped cavities with novel obstacles

Alireza Aghaei<sup>a</sup>, Suvanjan Bhattacharyya<sup>b</sup>, Amin Dezfulzadeh<sup>c</sup>, A.S. Goldanlou<sup>d</sup>, S. Rostami<sup>d</sup> and Mohsen Sharifpur<sup>e,f,g</sup>

<sup>a</sup>Department of Mechanical Engineering, University of Kashan, Kashan, Iran; <sup>b</sup>Department of Mechanical Engineering, Birla Institute of Technology and Science, Pilani, India; <sup>c</sup>Department of Mechanical Engineering, Arak Branch, Islamic Azad University, Arak, Iran; <sup>d</sup>Independent researcher; <sup>e</sup>Department of Mechanical Engineering, University of Science and Culture, Tehran, Iran; <sup>f</sup>Department of Medical Research, China Medical University Hospital, China Medical University, Taichung, Taiwan; <sup>g</sup>Department of Mechanical and Aeronautical Engineering, University of Pretoria, Pretoria, South Africa

## ABSTRACT

This work computationally explores the two-phase flow of nanofluids and their thermal energy transport coefficients in 3D diamond-shaped cavities with square-shaped barriers having reducing dimensions. Materials with two emissivity values,  $\varepsilon = 0.3$  and  $0.9$ , have been considered to investigate the effect of the radiation thermal energy transport coefficient while the hot side is maintained at 400 or 500 K. Two values of the Rayleigh number,  $Ra = 10^6$  and  $10^8$ , are used for the study. Cu nanoparticles (NPs) with an average size of 25 nm have been used at a concentration of 0.01–0.05% in the base fluid. The temperature gradients and thermal energy transport coefficient characteristics are enhanced by raising the volume concentration of nanoparticles, but the streamlines do not alter substantially. By increasing  $Ra$ , the thermal energy transport coefficient rate is further augmented. It is also found that increasing the  $Ra$  and volume concentration of NPs results in enhanced heat transfer inside a cavity, while a change in the emissivity coefficient has no significant impact on the thermal and flow characteristics of the nanofluid. For each case, there is an optimum NP volume fraction for each model that leads to the highest Nusselt number.

## ARTICLE HISTORY

Received 14 June 2020  
Accepted 3 May 2021

## KEYWORDS

Steady-state; natural convection; two-phase; nanofluid; heat transfer

## 1. Introduction

Developing energy concerns have encouraged the expansion of novel models for the utilization of high-performance heat exchangers (HEs). Nowadays, electronic cooling heat exchangers (ECHEs) that are used in fast all-electric systems and computing applications, and using nanofluids (NFs) to achieve a higher heat transfer (HT) coefficient, have been investigated by several authors for increased thermal performance. Furthermore, nanofluids have recently been at the center of attention because of their accurate thermophysical properties.

Khodabandeh et al. (2020) studied numerically the thermohydraulic characteristics of  $H_2O$ –silver NF in a spiral HE. The objective of this work is to improve the HT performance of an HE using two-phase NFs. The results show that, with an increase in the volume fraction of nanoparticles (NPs), the HT increases but at the same time the pressure drop (PD) penalty increases with the increase of spiral rotation and velocity of the working fluid.

He et al. (2020) investigated computationally the influence of a swirl generator on the thermohydraulic characteristics of a  $H_2O$ – $CuO$  NF inside a tube. The objective of the work was to explore a swirl generator effect on the performance of HT by using NFs. An interesting outcome reported by the investigators was that, by using a helical swirl generator and the NFs studied, the thermohydraulic performance was enhanced by 18.2%.

Computational studies were performed by Barnoon et al. (2019) on different NFs ( $H_2O$ – $Al_2O_3$ ,  $H_2O$ – $SiO_2$ ,  $H_2O$ – $ZnO$  and  $H_2O$ – $TiO_2$ ) to investigate entropy generation in the presence of a magnetic field. The results showed that increasing the diameter of the NPs increased the wall temperature and produced entropy. Also, by increasing the Hartmann number, the entropy produced increased.

Mashayekhi et al. (2017) studied computationally the influence of a conical strip on the thermohydraulic characteristics of a  $H_2O$ –silver NF in a tube. The outcome illustrated that, by using conical strip spiral turbulators, the average Nusselt number ( $Nu$ ) and friction

factor ( $f$ ) increased significantly compared to the base case.

Siavashi et al. (2017) studied computationally the influence of a porous type swirl generator on the thermohydraulic characteristics of an  $H_2O-Al_2O_3$  NF in a two-phase channel. The outcomes demonstrated that the tooth height and porous setting had a significant influence on the HT performance.

Alsarraf et al. (2019) studied computationally the influence of alumina NPs on HT and PD in a two-phase HE. The results showed that the shapes of spherical and platelet nanoparticles had the highest and lowest HT performance in the HE, respectively.

Varzaneh et al. (2020) studied computationally the influence of a ribbed micro-tube on the thermohydraulic characteristics of an alumina NF. The effects demonstrated that, by using rib roughness, the thermohydraulic performance rose by about 19%.

Milani Shirvan et al. (2017) investigated computationally the influence of an  $Al_2O_3$  aluminum water-oxide NF in a two-tube HE using a two-phase model. The results showed that, with increasing Reynolds number ( $Re$ ), the average  $Nu$  increased.

Samadifar and Toghraie (2018) studied computationally the influence of vortex generators on the flow field and HT in HEs having triangular cross sections. Their results showed that the use of rectangular vortex generators increased HT more than other vortex generators.

Xu et al. (2017) studied computationally the influence of vortex generators on the flow field and HT within a circular tube with constant heat flux. Their results showed that the maximum HT was achieved with an angle of attack of  $45^\circ$  when the obstruction ratio was 0.3. Also, as the instability increased, the HT and the coefficient of friction increased.

Sheikholeslami et al. (2020) made a numerical study of turbulator generated entropy on the flow field and HT of water-copper oxide NFs by considering a two-phase model in a solar system. Their results show that the greatest decrease in entropy production with increasing  $Re$  occurred when using a twisted barrier.

Some researchers (Alsabery et al., 2019; Alsabery, Gedik, et al., 2020; Alsabery, Ismael, et al., 2020; Ayoubi Ayoubloo et al., 2019; Chamkha et al., 2019; Dogonchi et al., 2020; Hoseinzadeh et al., 2019; Mehryan, Izadi, et al., 2019; Mehryan, Izadpanahi, et al., 2019; Selimefendigil et al., 2019; Shashikumar et al., 2019; Tayebi et al., 2019) have studied the thermohydraulic characteristics numerically through circular and non-circular tubes by using various single acting NFs and hybrid NFs. Also, some others researchers (Aghayari et al., 2020; Ahmadi et al., 2020; Beigzadeh et al., 2020; Ez Abadi et al., 2020; Gan et al., 2020; Ghahremannezhad et al., 2019; Jilte et al.,

2020; Maddah et al., 2019; Sharma et al., 2020) explored, both experimentally and computationally, the thermal performance of NFs in micro, mini and conventional circular and non-circular channels. Similarly, Mahdavi et al. (2017), Neyestani et al. (2019) and Sharifpur et al. (2018) studied, both experimentally and numerically, natural and forced convection by using newly developed nanofluids.

After reviewing the available literature based on the effect of using NFs in electrical heat exchangers, the present authors found that no study had investigated NF flow and HT in a 3D diamond-shaped cavity fitted with a square-shaped barrier having reducing dimensions. Therefore, the chief objective of the present work is to investigate numerically the influence of the emissivity of the material, the Rayleigh number ( $Ra$ ), and the volume fraction of NPs on the thermal and flow characteristics of a 3D diamond-shaped cavity (DSC) fitted with a square-shaped barrier having reducing dimensions. ANSYS<sup>®</sup>-Fluent<sup>®</sup> 15.0 was used for the solution to the boundary-value problem, and the SolidWorks<sup>®</sup> and ANSYS<sup>®</sup>-Workbench software packages were used for the creation of the mesh considered.

## 2. Methodology

### 2.1. Model

Figures 1 and 2 illustrate the schematic of a basic 3D DSC fitted with a square-shaped obstacle having reducing dimensions. The diamond height is varied from 173.10 to 283.93 mm, and the length of the diamond is 1000 mm. Also, the square height is varied from 46.03 to 70.71 mm ( $L_{\text{square}} = 1000$  mm). The system is made of stainless steel 304 of 2.0 mm thickness ( $\varepsilon = 0.3$  and  $\varepsilon = 0.9$ );  $Ra = 10^6$  and  $10^8$ . It is very clear that, in the present study,  $Ra$  is in the turbulent regime ( $T_{\text{initial}} = 350$  K,  $T_c = 280$  K,  $T_h = 400$  or  $500$  K). The HT fluid is a water-Cu NF, which creates a Newtonian NF, with concentrations ( $\phi$ ) of 0.01–0.05%. Table 1 reports the important properties of the Newtonian base fluid and solid particles.

Assumptions: (1) the problem is steady state; (2) the flow regime is turbulent; (3) the fluid flow is incompressible; (4) the nanofluid has Newtonian behavior; and (5) the nanofluid is two phase.

**Table 1.** Thermophysical properties (Aladdin et al., 2020).

Fluid	$k$ (W/m·K)	$c_p$ (J/kg·K)	$\rho$ (kg/m <sup>3</sup> )
Cu	400	385	8933
H <sub>2</sub> O	0.613	4179	997.1

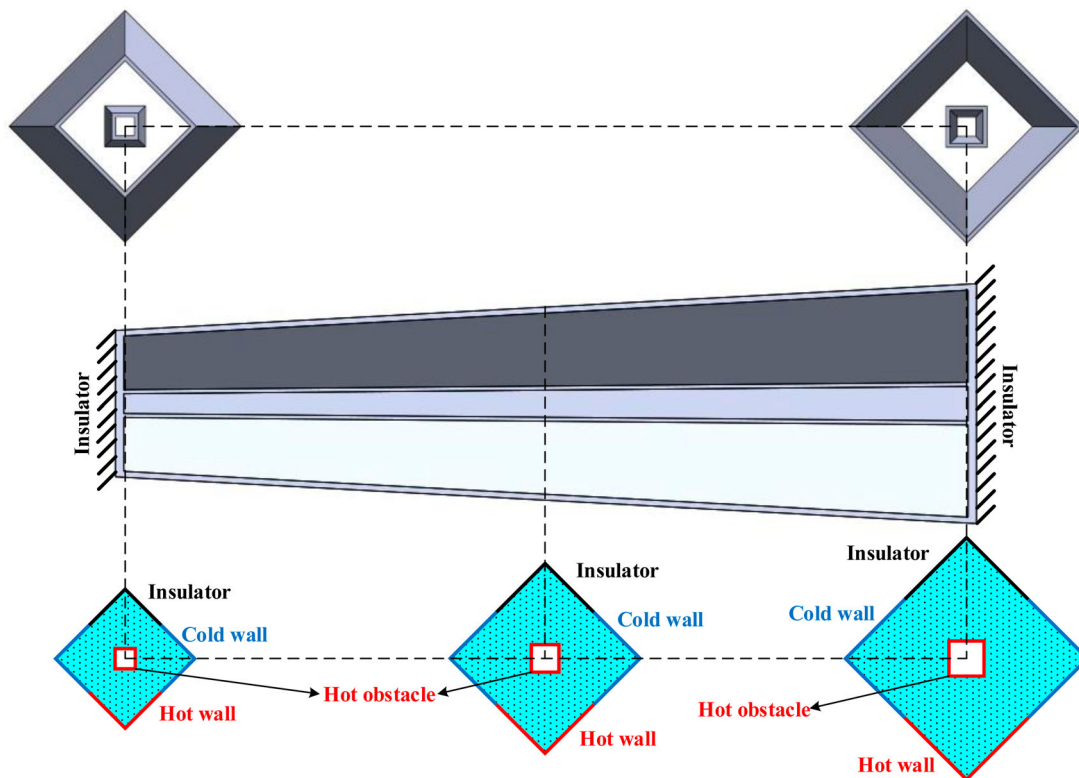


**Figure 1.** Schematic diagrams of the basic geometry in the present paper.

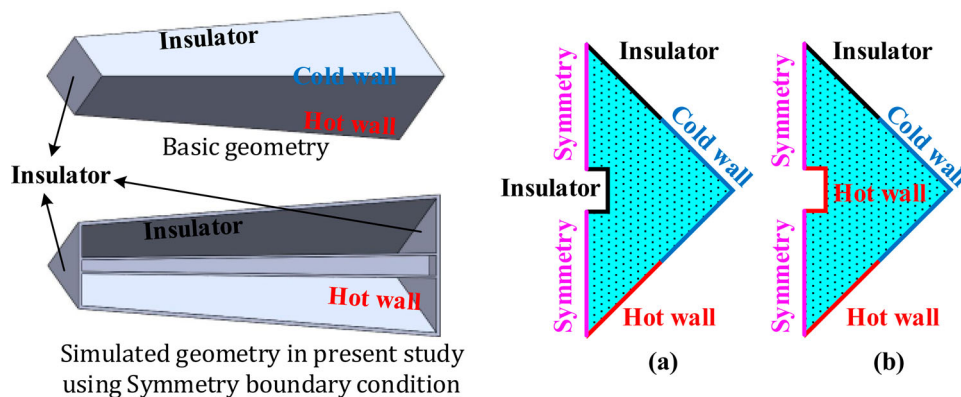


**Figure 2.** Schematic diagrams of the geometry studied in the present work and boundary conditions.

The effective density  $\rho_{nf}$  and specific heat  $c_{p,nf}$  of the NF at each section-temperature ( $T_m$ ) are calculated using the equations of Kim et al. (2009). Also, the thermal conductivity ( $k$ ) can be calculated using the equations in Table 2. By considering the Brownian motion of nanoparticles and employing the equations of Corcione (2011) in a 3D cavity, the NF thermal conductivity can be obtained, where  $Re_{np}$  is the Re of the NPs, the Prandtl number (Pr) is that of the base liquid,  $T$  is the temperature of the nanofluid,  $T_{fr}$  is the base liquid freezing point,  $k_{np}$  is the thermal/heat conductivity of NPs, and  $\phi$  is the suspended nanoparticle volume fraction. The Re of the NPs is calculated from Table 2 (Corcione, 2011), where  $\rho_{bf}$  and  $\mu_{bf}$  are the base fluid

density and the dynamic viscosity, and  $d_{np}$  and  $u_B$  are the nanoparticle size and average Brownian velocity, respectively. Considering no agglomeration, the NPs' Brownian velocity  $u_B$  can attain as  $d_{np}$  and  $\tau_D$  ratio obligatory to shelter such distance (Corcione, 2011), where  $D$  is the self-diffusion coefficient and  $k_b$  is Boltzmann's constant (Corcione, 2011). Note that in the earlier equations all the physical properties were calculated at the NF temperature  $T$ . Also, the dynamic viscosity was calculated from Table 2 (Corcione, 2011), where  $M$  is the molar weight of the base fluid,  $N$  is Avogadro's number, and  $\rho_{f0}$  is the density of the base fluid calculated at  $T_0 = 293K$ , where  $d_{bf}$  is the equivalent diameter of a base fluid molecule (Corcione, 2011).

**Table 2.** Equations used in this study (Aladdin et al., 2020; Corcione, 2011).

Density	$\rho_{nf} = \phi_{np}\rho_{np} + (1 - \phi_{np})\rho_{bf}$
Specific heat	$c_{p,nf} = \phi_{np}c_{p,np} + (1 - \phi_{np})c_{p,bf}$
Thermal conductivity	$\frac{k_{eff}}{k_{bf}} = 1 + 4.4Re_{np}^{0.4}Pr_{bf}^{0.66}\phi^{0.66}\left(\frac{T}{T_f}\right)^{10}\left(\frac{k_{np}}{k_{bf}}\right)^{0.03}$ $Re_{np} = \frac{\rho_{bf}u_B d_{np}}{\mu_{bf}}$ $\tau_D = \frac{d_{np}^2}{6D} = \frac{\pi\mu_{bf}d_{np}^3}{2k_b T}$ $u_B = \frac{2k_b T}{\pi\mu_{bf}d_{np}^2}$ $Re_{np} = \frac{2\rho_{bf}k_b T}{\pi\mu_{bf}^2 d_{np}}$
Dynamic viscosity	$\frac{\mu_{eff}}{\mu_{bf}} = \frac{1}{1 - 34.87\left(\frac{d_{np}}{d_{bf}}\right)^{-0.3}\phi^{1.03}}$ $d_{bf} = 0.1\left(\frac{6M}{N\pi\rho_{f0}}\right)^{\frac{1}{3}}$

The symmetry conditions

- fluxes across the symmetry = 0
- normal components of all variables = 0

can be applied to both planar or non-planar faces/surfaces on the domain boundaries.

To compute the NF flow through a cylinder, the two-phase flow method is engaged and presented in Table 3. The equations of continuity, energy and momentum are also presented in Table 3 (Al-Ansary & Zeitoun, 2011; Arani et al., 2017; Heris et al., 2012; Kim et al., 2009; Patankar, 1980; Sadripour, 2019; Sadripour & Chamkha, 2019; Salari et al., 2020). The volume fraction/concentration equation for a two-phase mixture and the slip velocity are also in Table 3 (Al-Ansary & Zeitoun, 2011; Aladdin et al., 2020; Arani et al., 2017; Corcione, 2011; Heris et al., 2012; Karami et al., 2020; Karimi et al.,

2019; Kim et al., 2009; Patankar, 1980; Sadripour, 2019; Sadripour & Chamkha, 2019; Salari et al., 2020). The NFs' Re is also calculated using the equations in Table 3, where  $d_p$  is the mean particle diameter. The equations that describe the  $k-\epsilon$  model are also reported in Table 3, where the turbulent dynamic viscosity is  $\mu_{t,m}$  and the production rate of  $k$  is  $G$  (Ahmadi et al., 2019; Karimi et al., 2019; Vatani & Mohammed, 2013). The standard constants  $c_1 = 1.44, C_\mu = 0.09, \sigma_k = 1.00, c_2 = 1.92, \sigma_\epsilon = 0.85$  and  $\sigma_\epsilon = 1.30$  are used, and the Ra and Nu of the nanofluid are also reported in Table 3 (Karimi et al., 2019).

## 2.2. Validation

### 2.2.1. Mesh independency test

A grid independency study is an important study in the numerical analysis (Baghban et al., 2019; Fereidoon et al., 2013; Ghalandari et al., 2019; Heris et al., 2012; Ramezanizadeh et al., 2019). Figure 3 shows a grid independence test (GIT) performed for the studied cavity filled with NF to explore the influences of grid size on the results for the grid mesh generated.

### 2.2.2. Code validation

The other important issue is to validate the employed computer code using available validated numerical or experimental papers in the literature. Figure 4 illustrates the validation of the current work with the results obtained by Leong et al. (1998) and Giwa et al. (2020) in cases where Nu is a function of Ra. Giwa et al. (2020) studied experimentally the convection HT characteristics of a differentially heated square-shaped cavity filled with

**Table 3.** Governing equations and important parameters (Al-Ansary & Zeitoun, 2011; Arani et al., 2017; Patankar, 1980; Sadripour, 2019; Sadripour & Chamkha, 2019; Salari et al., 2020).

Continuity equation	$\nabla(\rho_m \vec{U}_m) = 0$ $\vec{U}_m = \frac{\rho_s \phi_s \vec{U}_s + \rho_{bf} \phi_{bf} \vec{U}_{bf}}{\rho_m}$ $\rho_m = \rho_s \phi_s + \rho_{bf} \phi_{bf}$
Momentum equation	$\rho_m(\vec{U}_m \nabla \vec{U}_m) = -\nabla \vec{P} + \mu_m(\nabla \vec{U}_m + (\nabla \vec{U}_m)^T) + \nabla(\rho_{bf} \phi_{bf} \vec{U}_{dr,bf} \vec{U}_{dr,bf} + \rho_s \phi_s \vec{U}_{dr,s} \vec{U}_{dr,s}) + \rho_m \vec{g}$ $\vec{U}_{dr,bf} = \vec{U}_{bf} - \vec{U}_m$ $\vec{U}_{dr,s} = \vec{U}_s - \vec{U}_m$
Energy equation	$\nabla(\rho_{bf} \phi_{bf} \vec{U}_{bf} h_{bf} + \rho_s \phi_s \vec{U}_s h_s) = \nabla((\phi_{bf} k_{bf} + \phi_s k_s) \nabla \vec{T})$ $\nabla(\rho_s \phi_s \vec{U}_m) = -\nabla(\rho_s \phi_s \vec{U}_{dr,s})$ $\vec{U}_{bf,s} = \vec{U}_{bf} - \vec{U}_s$ $\vec{U}_{dr,s} = \vec{U}_s - \frac{\rho_s \phi_s}{\rho_m} \vec{U}_{bf,s}$ $\vec{U}_{bf,s} = \frac{d_p^2}{18\mu_{bf} \tau_d} \frac{\rho_s - \rho_m}{\rho_s} \vec{\alpha}$ $f_d = 1 + 0.15 Re_s^{0.687}$ $\vec{\alpha} = \vec{g} - (\vec{U}_m \nabla \vec{U}_m)$ $Re_s = \frac{\vec{U}_m d_p \rho_m}{\mu_m}$
Turbulence equations	$\nabla(\rho_m \vec{U}_m k) = \nabla \left[ \left( \mu_m + \frac{\mu_{t,m}}{\sigma_k} \right) \nabla k \right] + G_{k,m} - \rho_m \epsilon$ $\nabla(\rho_m \vec{U}_m \epsilon) = \nabla \left[ \left( \mu_m + \frac{\mu_{t,m}}{\sigma_\epsilon} \right) \nabla \epsilon \right] + \frac{\epsilon}{k} (c_1 G_{k,m} - c_2 \rho_m \epsilon)$ $\mu_{t,m} = C_\mu \rho_m \frac{k^2}{\epsilon}$ $G_{k,m} = \mu_{t,m} (\nabla \vec{U}_m + (\nabla \vec{U}_m)^T)$
Parameters of interest	$Ra = \frac{8g\beta(T_h - T_c)}{d_{bf} \alpha_{bf}} Nu = \frac{k_{nf}}{k_f} \int \frac{\partial T}{\partial x}$



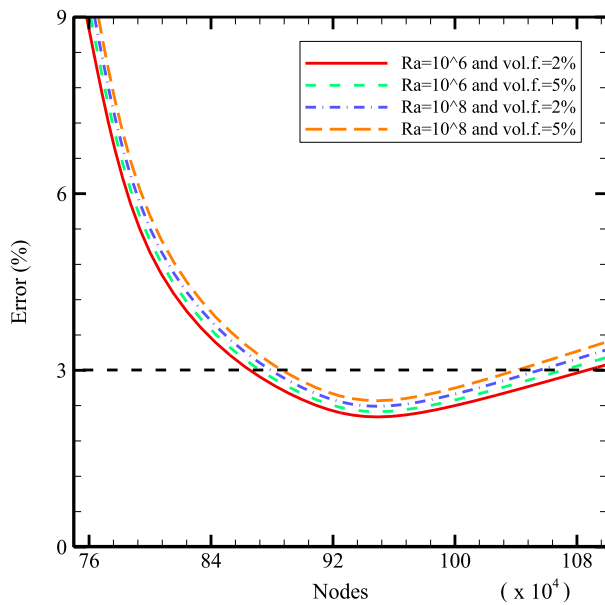


**Figure 3.** Mesh independency test.

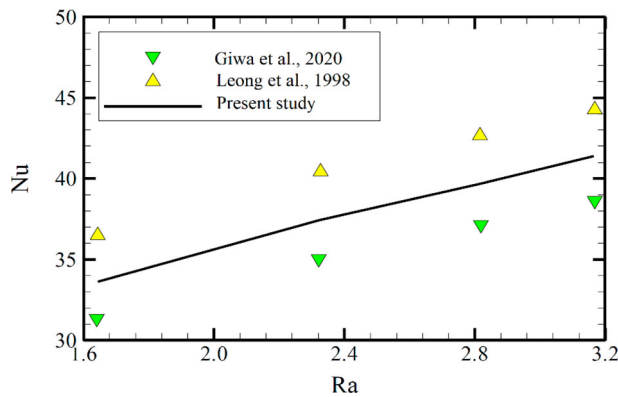


**Figure 4.** Validation of current study with the results obtained by Leong et al. (1998) and Giwa et al. (2020) in the case of Nu versus different Ra's.

an  $\text{Al}_2\text{O}_3$ -MWCNT/water NF. Also, Leong et al. (1998) conducted an experimental study to investigate the natural convection HT performance of a cubic-shaped cavity.

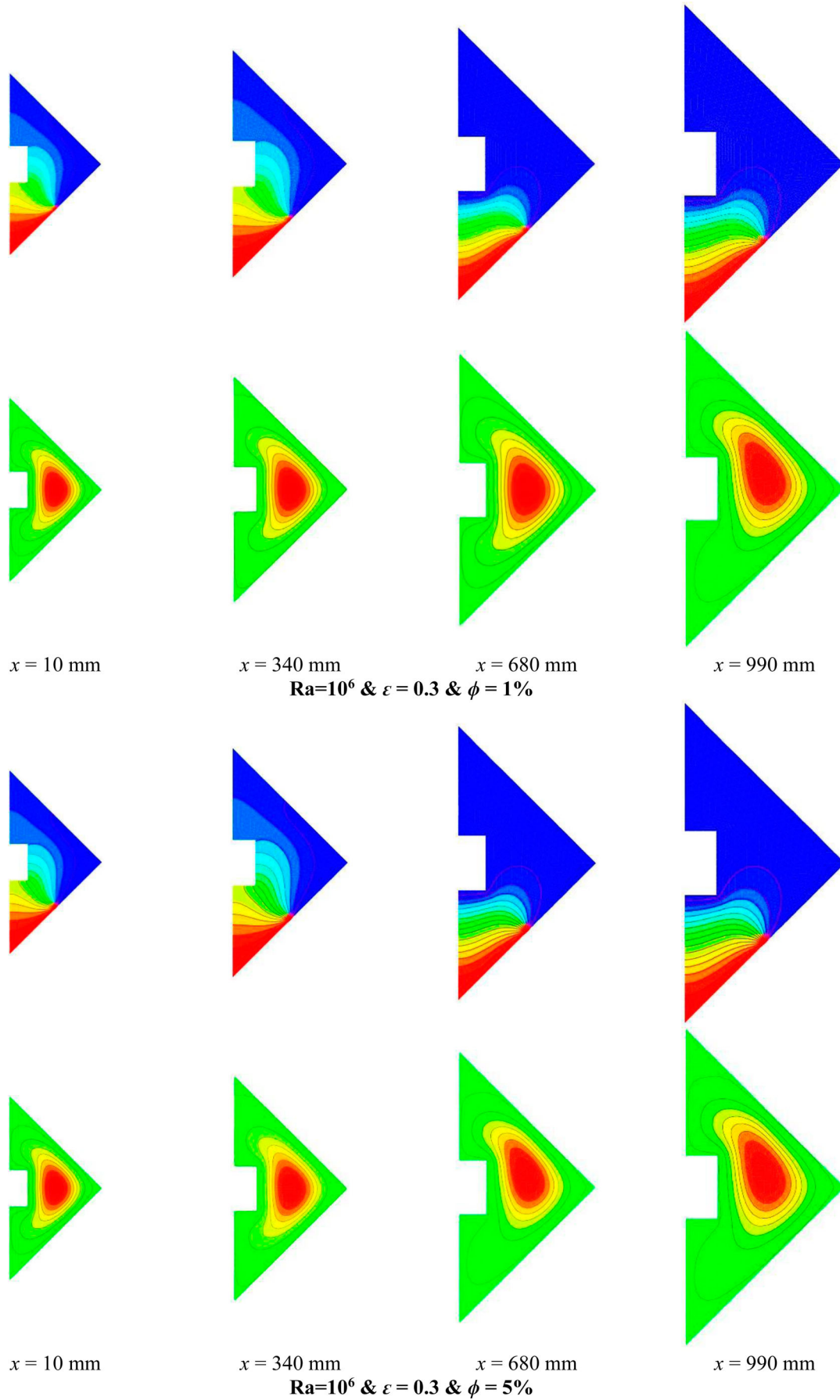
### 3. Results and discussion

NF flow has a higher thermal conductivity than the base fluid and can transfer more energy. But the nanofluid also has more dynamic viscosity than the base fluid, which increases the PD penalty and  $f$  in the system. However, in the present system a pressure drop does not matter. Figure 5 illustrates the temperature and velocity contours for various nanoparticle volume fractions and at various cross sections of a 3D cavity with  $\varepsilon = 0.3$  and  $\text{Ra} = 10^6$  for a case with  $T_h = 400$  K and an insulator obstacle. As shown in this figure, on the left-hand side of the cavity,

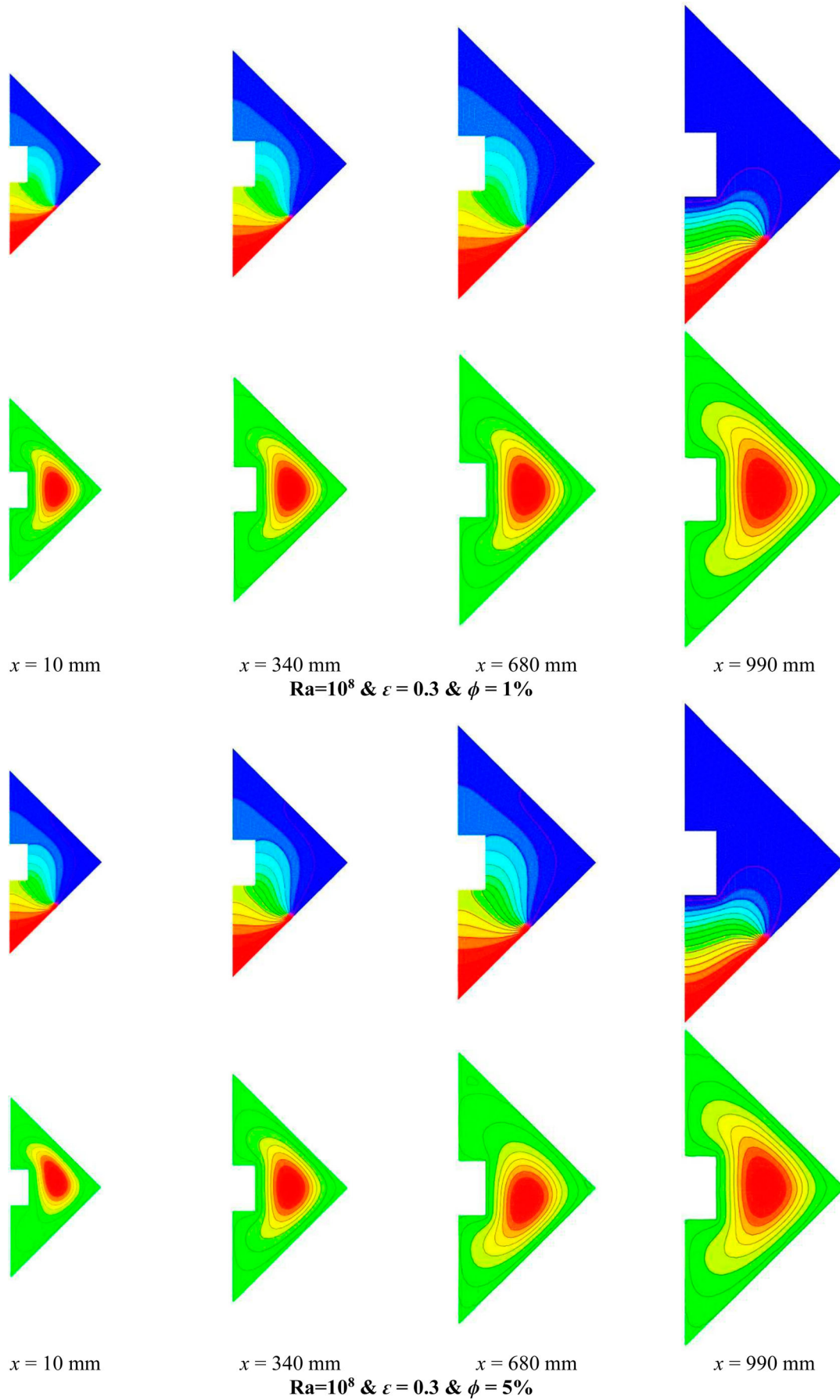
which has smaller dimensions, the HT characteristics are stronger. Also, it is seen that, in all cases, a non-clockwise vortex exists in the cavity because of temperature gradients. It is also realized that, by raising the NPs'  $\phi$ , the temperature gradients and HT behavior are better, but the streamlines do not show any noteworthy change. Figure 6 illustrates the temperature and velocity contours for various nanoparticle volume fractions and at various cross sections of a 3D cavity with  $\varepsilon = 0.3$  and  $\text{Ra} = 10^8$  for a case with  $T_h = 400$  K and an insulator obstacle. Also, by comparing Figures 5 and 6, it is realized that, at higher Ra, the HT characteristics are augmented. Figure 7 illustrates the temperature and velocity contours for various nanoparticle volume fractions and at various cross sections of a 3D cavity with  $\varepsilon = 0.3$  and  $\text{Ra} = 10^6$  for a case with  $T_h = 400$  K and a heated obstacle. As shown in this figure, on the left-hand side of the cavity, which has smaller dimensions, the HT characteristics are stronger. Additionally, it is seen that, in all cases, a non-clockwise vortex exists in the cavity because of temperature gradients. It is also realized that, by raising the NPs'  $\phi$ , the temperature gradients and HT behavior are better, but the streamlines do not show any noteworthy change. Figure 8 illustrates the temperature and velocity contours for various nanoparticle volume fractions and at various cross sections of a 3D cavity with  $\varepsilon = 0.3$  and  $\text{Ra} = 10^8$  for a case with  $T_h = 400$  K and a heated obstacle. As shown in this figure, on the left-hand side of the cavity, which has smaller dimensions, the HT characteristics are stronger. Also, it is seen that, in all cases, a non-clockwise vortex exists in the cavity because of temperature gradients. It is also realized that, by raising the NPs'  $\phi$ , the temperature gradients and HT behavior are better, but the streamlines do not show any noteworthy change. The HT rate is always raised by increasing Ra. Higher Rayleigh numbers lead to more turbulent flow and more vortex generation in the system, which increase the flow mixing rate in channels. This leads to a higher HT coefficient and increases the HT rate in the system.

Figure 9 illustrates the temperature and velocity contours for various nanoparticle volume fractions and at various cross sections of a 3D cavity with  $\varepsilon = 0.3$  and  $\text{Ra} = 10^6$  for a case with  $T_h = 500$  K and a heated obstacle. As shown in this figure, on the left-hand side of the cavity, which has smaller dimensions, the HT characteristics are stronger. Also, it is seen that, in all cases, a clockwise and also a non-clockwise vortex exist in the cavity because of temperature gradients. It is also realized that, by raising the NPs'  $\phi$ , the temperature gradients and HT behavior are better.

Figure 10 illustrates the temperature and velocity contours for various nanoparticle volume fractions and at various cross sections of a 3D cavity with  $\varepsilon = 0.3$  and



**Figure 5.** Temperature and velocity contours for various nanoparticle volume fractions and at various cross sections of a 3D cavity with  $\varepsilon = 0.3$  and  $\text{Ra} = 10^6$  for a case with  $T_h = 400 \text{ K}$  and an insulator obstacle.



**Figure 6.** Temperature and velocity contours for various nanoparticle volume fractions and at various cross sections of a 3D cavity with  $\varepsilon = 0.3$  and  $Ra = 10^8$  for a case with  $T_h = 400$  K and an insulator obstacle.

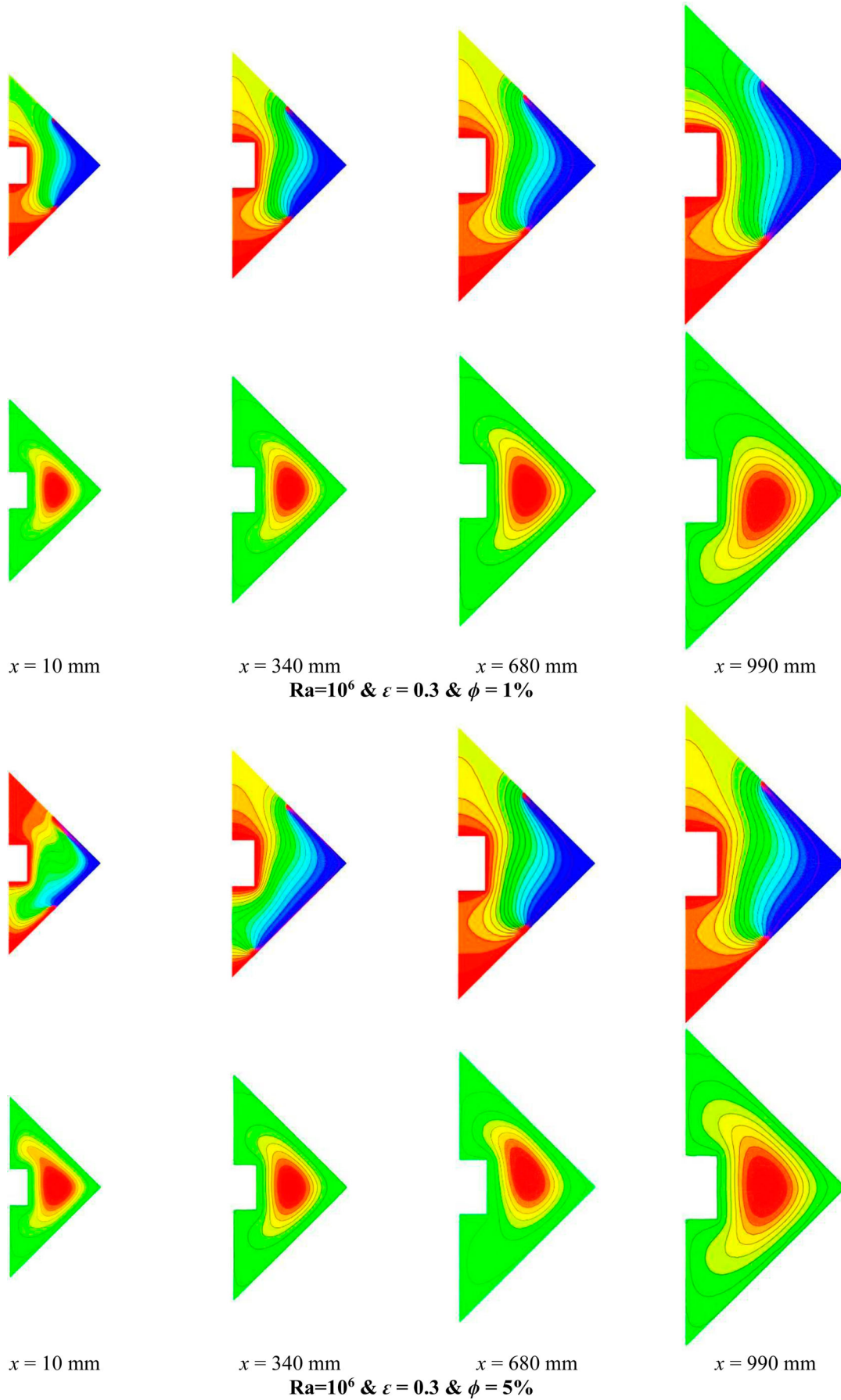


**Figure 7.** Temperature and velocity contours for various nanoparticle volume fractions and at various cross sections of a 3D cavity with  $\varepsilon = 0.3$  and  $Ra = 10^6$  for a case with  $T_h = 400 \text{ K}$  and a heated obstacle.



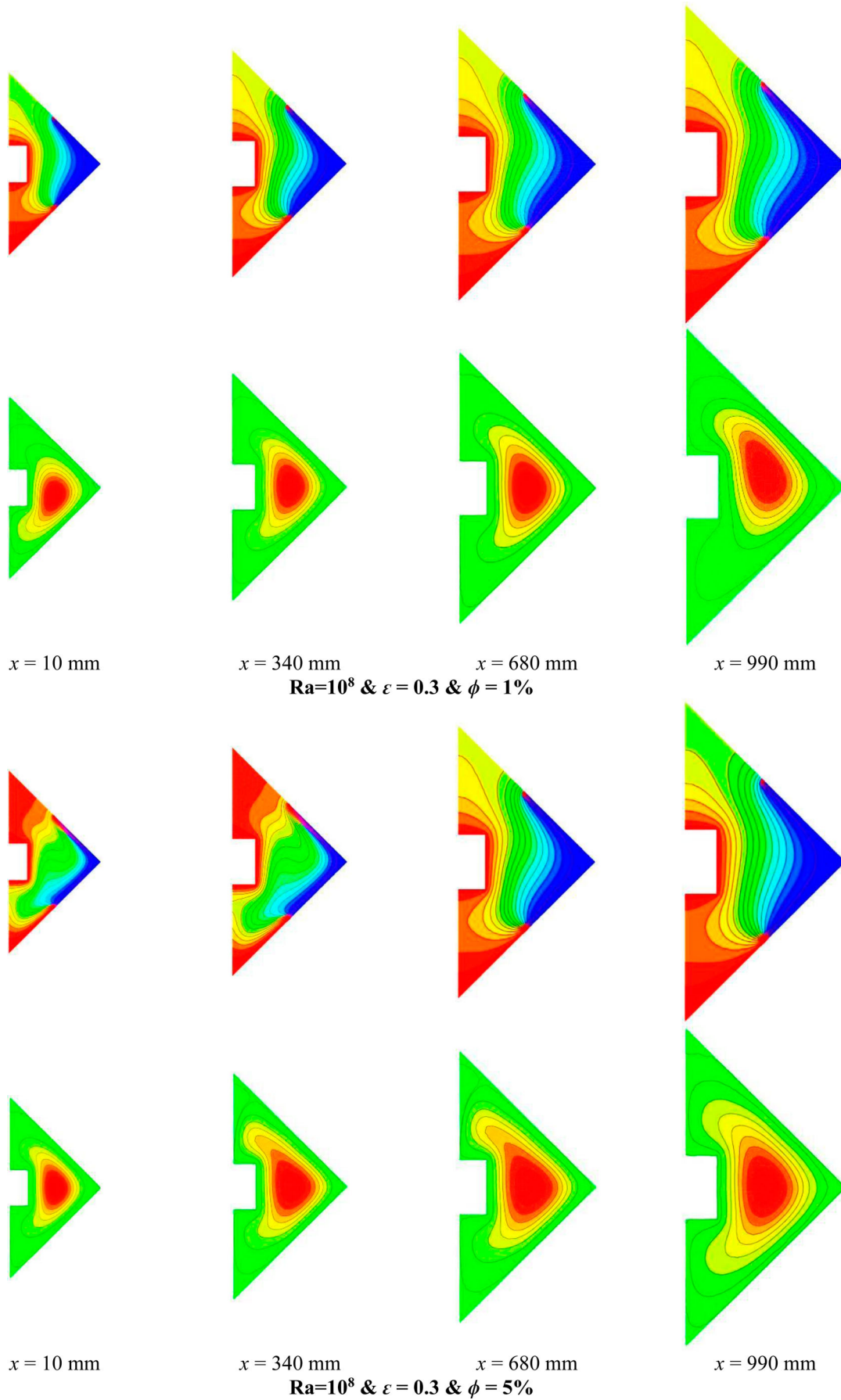


**Figure 8.** Temperature and velocity contours for various nanoparticle volume fractions and at various cross sections of a 3D cavity with  $\varepsilon = 0.3$  and  $\text{Ra} = 10^8$  for a case with  $T_h = 400$  K and a heated obstacle.

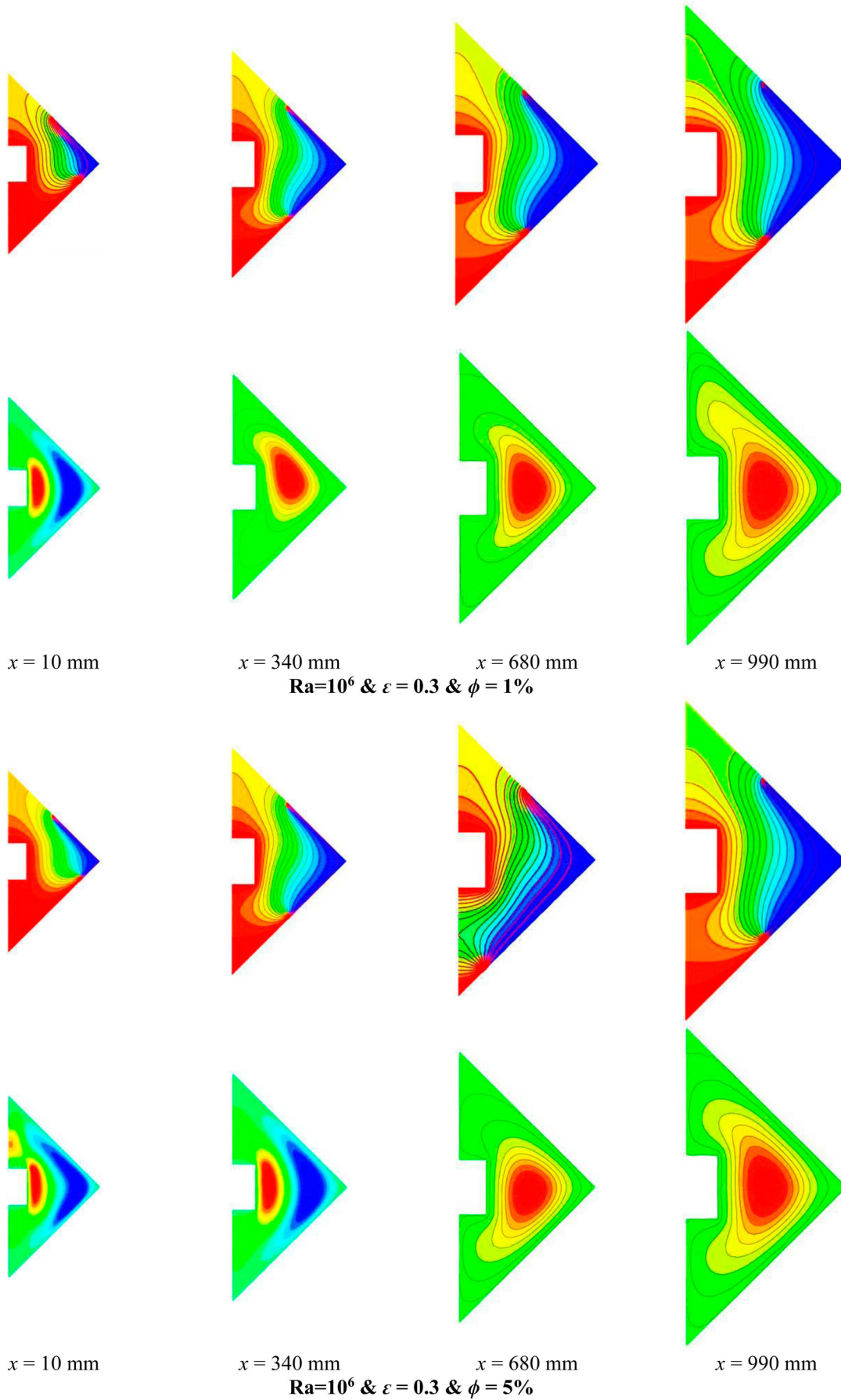


**Figure 9.** Temperature and velocity contours for various nanoparticle volume fractions and at various cross sections of a 3D cavity with  $\varepsilon = 0.3$  and  $Ra = 10^6$  for a case with  $T_h = 500 \text{ K}$  and a heated obstacle.

$Ra = 10^8$  for a case with  $T_h = 500$  K and a heated obstacle. As shown in this figure, on the left-hand side of the cavity, which has smaller dimensions, the HT characteristics are stronger. Also, it is seen that, in all cases, a clockwise and also a non-clockwise vortex exist in the cavity because of temperature gradients. It is also realized that, by raising the number of NPs  $\phi$ , the temperature gradients and HT behavior are better, but the streamlines do not show any noteworthy change. Also, by comparing Figures 9 and 10 it is realized that, at higher  $Ra$ , the HT characteristics are augmented. Therefore, it is realized that, in the case of using a material with an emissivity of 0.3, usage of a cavity with a heated obstacle and a constant hot-side temperature of 500 K should be suggested. Also, higher  $Ra$ 's and NPs'  $\phi$  lead to more HT inside the cavity.

Figure 11 illustrates the temperature and velocity contours for various nanoparticle volume fractions and at various cross sections of a 3D cavity with  $\varepsilon = 0.9$  and  $Ra = 10^6$  for a case with  $T_h = 400$  K and an insulator obstacle. As shown in this figure, on the left-hand side of the cavity, which has smaller dimensions, the HT characteristics are stronger. Furthermore, it is seen that, in all cases, a non-clockwise vortex exists in the cavity because of temperature gradients. It is also realized that, by raising the NPs'  $\phi$ , the temperature gradients and HT behavior are better. Figure 12 illustrates the temperature and velocity contours for various nanoparticle volume fractions and at various cross sections of a 3D cavity with  $\varepsilon = 0.9$  and  $Ra = 10^8$  for a case with  $T_h = 400$  K and an insulator obstacle. As shown in this figure, on the left-hand side of the cavity, which has smaller dimensions, the HT characteristics are stronger. Also, it is seen that, in all cases, a non-clockwise vortex exists in the cavity because of temperature gradients. It is also realized that, by raising the NPs'  $\phi$ , the temperature gradients and HT behavior are better, but the streamlines do not show any noteworthy change. Moreover, by comparing Figures 11 and 12, it is realized that, at higher  $Ra$ , the HT characteristics are augmented. A higher nanoparticle volume fraction leads to higher thermal conductivity and a higher Nusselt number.

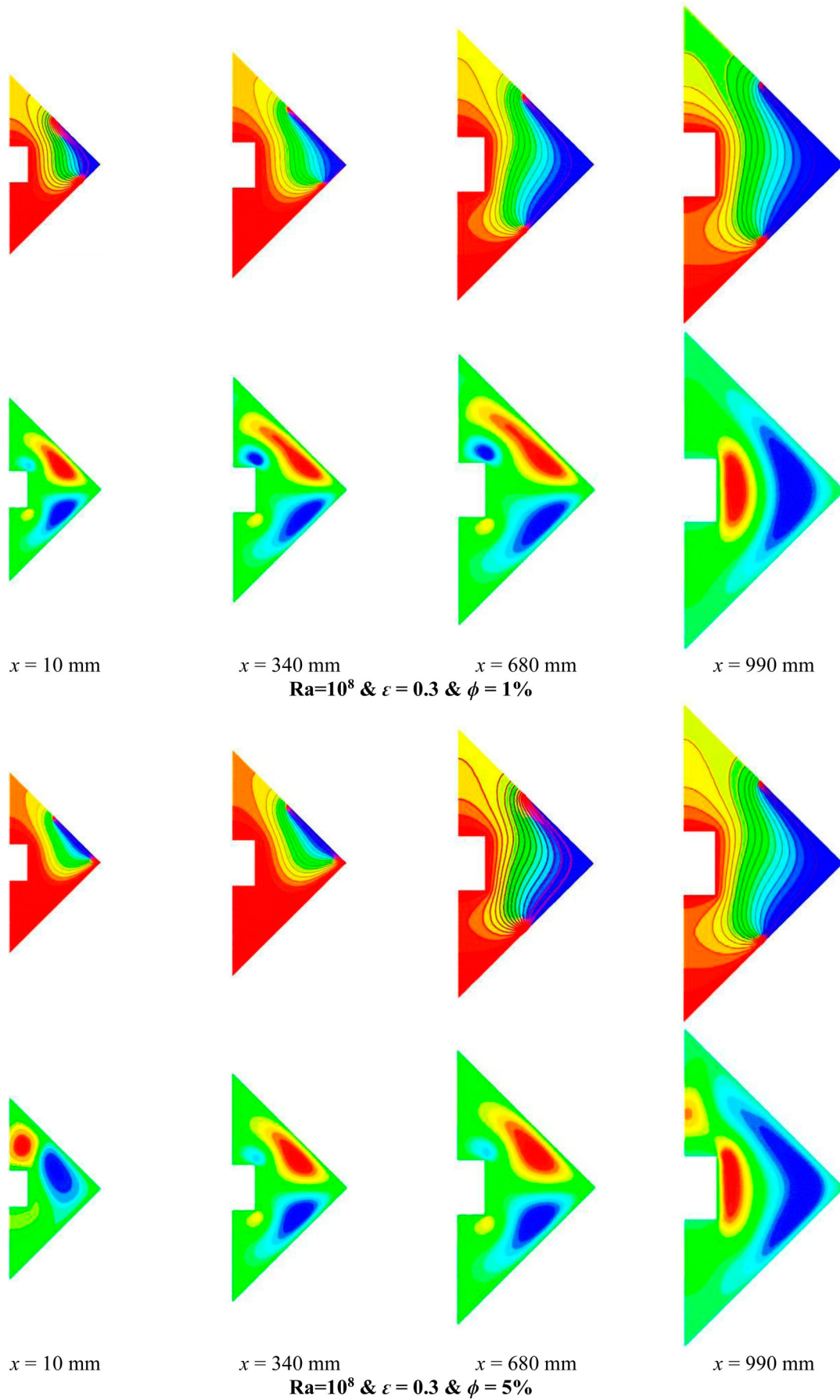
Figure 13 illustrates the temperature and velocity contours for various nanoparticle volume fractions and at various cross sections of a 3D cavity with  $\varepsilon = 0.9$  and  $Ra = 10^6$  for a case with  $T_h = 400$  K and a heated obstacle. As shown in this figure, on the left-hand side of the cavity, which has smaller dimensions, the HT characteristics are stronger. Also, it is seen that, in all cases, a non-clockwise vortex exists in the cavity because of temperature gradients. It is also realized that, by raising the NPs'  $\phi$ , the temperature gradients and HT behavior are better. Figure 14 illustrates the temperature and velocity

contours for various nanoparticle volume fractions and at various cross sections of a 3D cavity with  $\varepsilon = 0.9$  and  $Ra = 10^8$  for a case with  $T_h = 400$  K and a heated obstacle. As shown in this figure, on the left-hand side of the cavity, which has smaller dimensions, the HT characteristics are stronger. Also, it is seen that, in all cases, a non-clockwise vortex exists in the cavity because of temperature gradients. It is also realized that, by raising the NPs'  $\phi$ , the temperature gradients and HT behavior are better. Also, by comparing Figures 13 and 14, it is realized that, at higher  $Ra$ , the HT characteristics are augmented.

Figure 15 illustrates the temperature and velocity contours for various nanoparticle volume fractions and at various cross sections of a 3D cavity with  $\varepsilon = 0.9$  and  $Ra = 10^6$  for a case with  $T_h = 500$  K and a heated obstacle. As shown in this figure, on the left-hand side of the cavity, which has smaller dimensions, the HT characteristics are stronger. Also, it is seen that, in all cases, a clockwise and also a non-clockwise vortex exist in the cavity because of temperature gradients. It is also realized that, by raising the NPs'  $\phi$ , the temperature gradients and the HT behavior are better, but the streamlines do not show any noteworthy change.

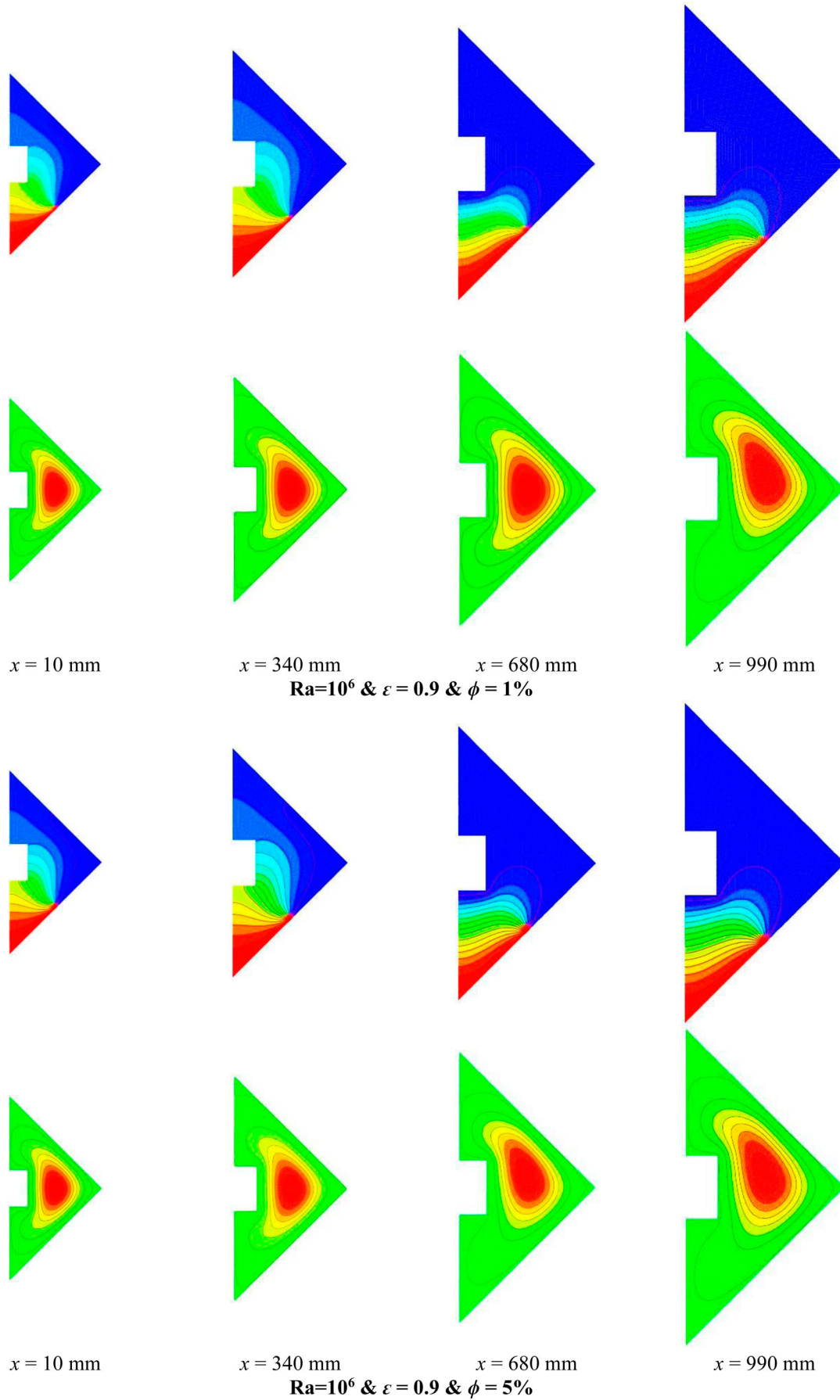
Figure 16 illustrates the temperature and velocity contours for various nanoparticle volume fractions and at various cross sections of a 3D cavity with  $\varepsilon = 0.9$  and  $Ra = 10^8$  for a case with  $T_h = 500$  K and a heated obstacle. As shown in this figure, on the left-hand side of the cavity, which has smaller dimensions, the HT characteristics are stronger. Also, it is seen that, in all cases, a clockwise and also a non-clockwise vortex exist in the cavity because of temperature gradients. It is also realized that, by raising the NPs'  $\phi$ , the temperature gradients and the HT behavior are better, but the streamlines do not show any noteworthy change. Also, by comparing Figures 15 and 16, it is realized that, at higher  $Ra$ , the HT characteristics are augmented. Therefore, it is realized that, in the case of using material with an emissivity of 0.9, usage of the cavity with a heated obstacle and a constant hot-side temperature of 500 K should be suggested. Also, higher  $Ra$  and NPs'  $\phi$  lead to more HT inside the cavity. It is also found that changes in the coefficients of emissivity do not show any noteworthy influence on the HT characteristics or NF flow in the cavity.

Figure 17 illustrates the predicted total average  $Nu$  versus different NP volume fractions  $\phi$  for different base fluids for a 3D cavity with  $\varepsilon = 0.3$  and  $Ra = 10^6$  and  $10^8$  for cases with  $T_h = 400$  and 500 K and a heated obstacle. As shown in Figure 17(a), for the case with  $Ra = 10^6$  and  $T_h = 400$ , the predicted average  $Nu$  is always raised by increasing the number of nanoparticles, and consequently, at an NP volume fraction of 0.05, the highest  $Nu$  is achieved. Also, it is realized that, for a case with water as



**Figure 10.** Temperature and velocity contours for various nanoparticle volume fractions and at various cross sections of a 3D cavity with  $\varepsilon = 0.3$  and  $\text{Ra} = 10^8$  for a case with  $T_h = 500$  K and a heated obstacle.





**Figure 11.** Temperature and velocity contours for various nanoparticle volume fractions and at various cross sections of a 3D cavity with  $\varepsilon = 0.9$  and  $Ra = 10^6$  for a case with  $T_h = 400 \text{ K}$  and an insulator obstacle.

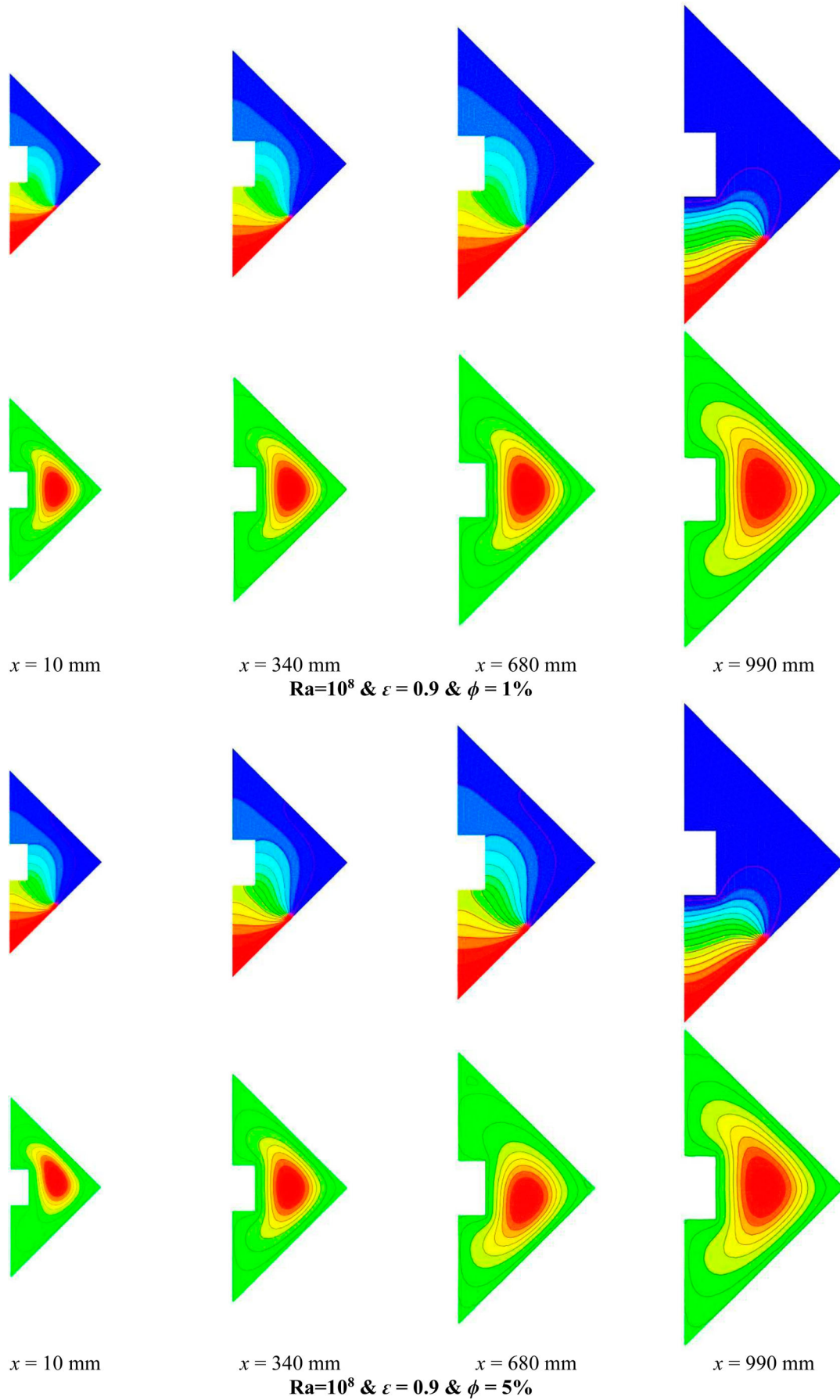


**Figure 12.** Temperature and velocity contours for various nanoparticle volume fractions and at various cross sections of a 3D cavity with  $\varepsilon = 0.9$  and  $Ra = 10^8$  for a case with  $T_h = 400 \text{ K}$  and an insulator obstacle.

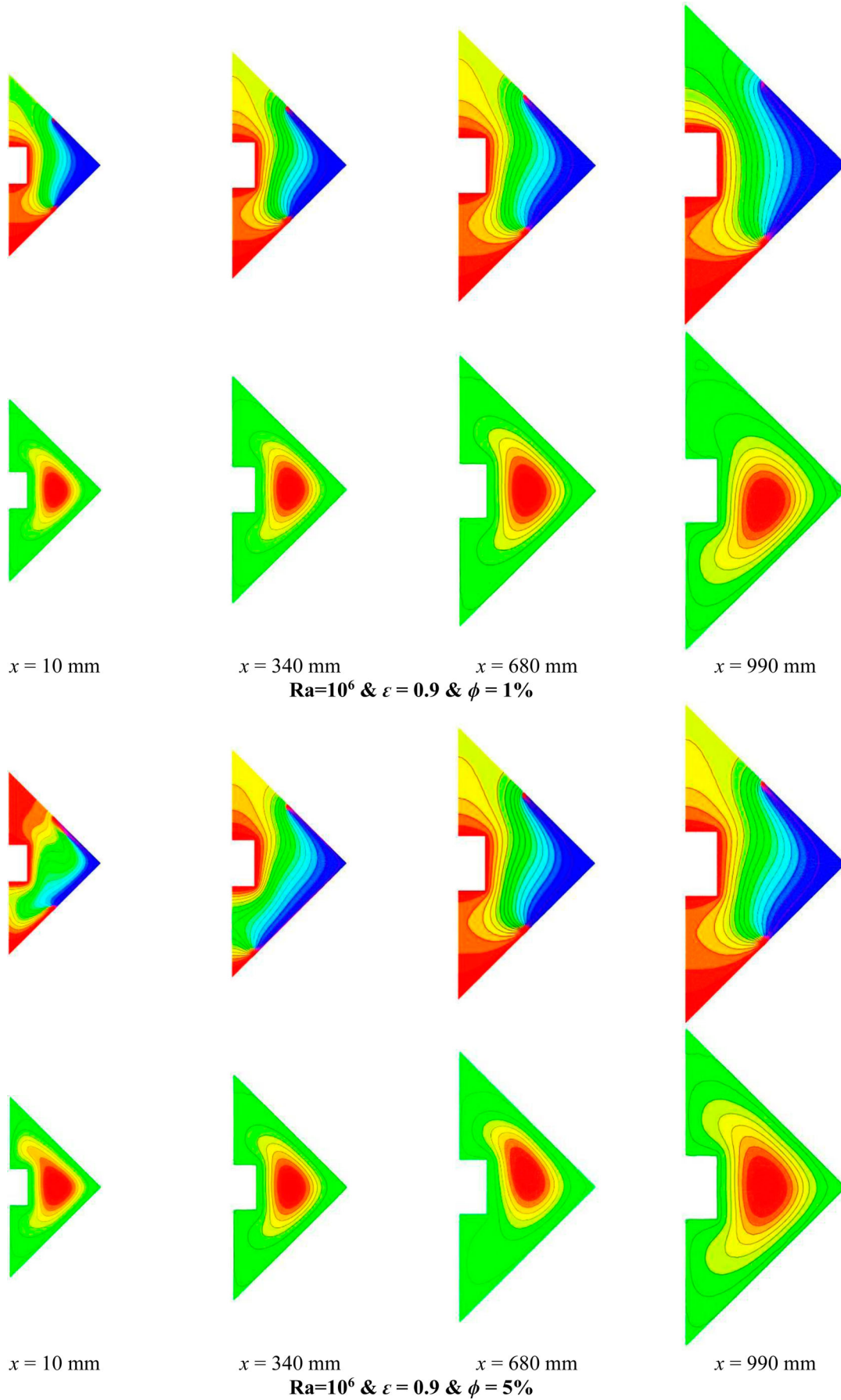


**Figure 13.** Temperature and velocity contours for various nanoparticle volume fractions and at various cross sections of a 3D cavity with  $\varepsilon = 0.9$  and  $Ra = 10^6$  for a case with  $T_h = 400 \text{ K}$  and a heated obstacle.

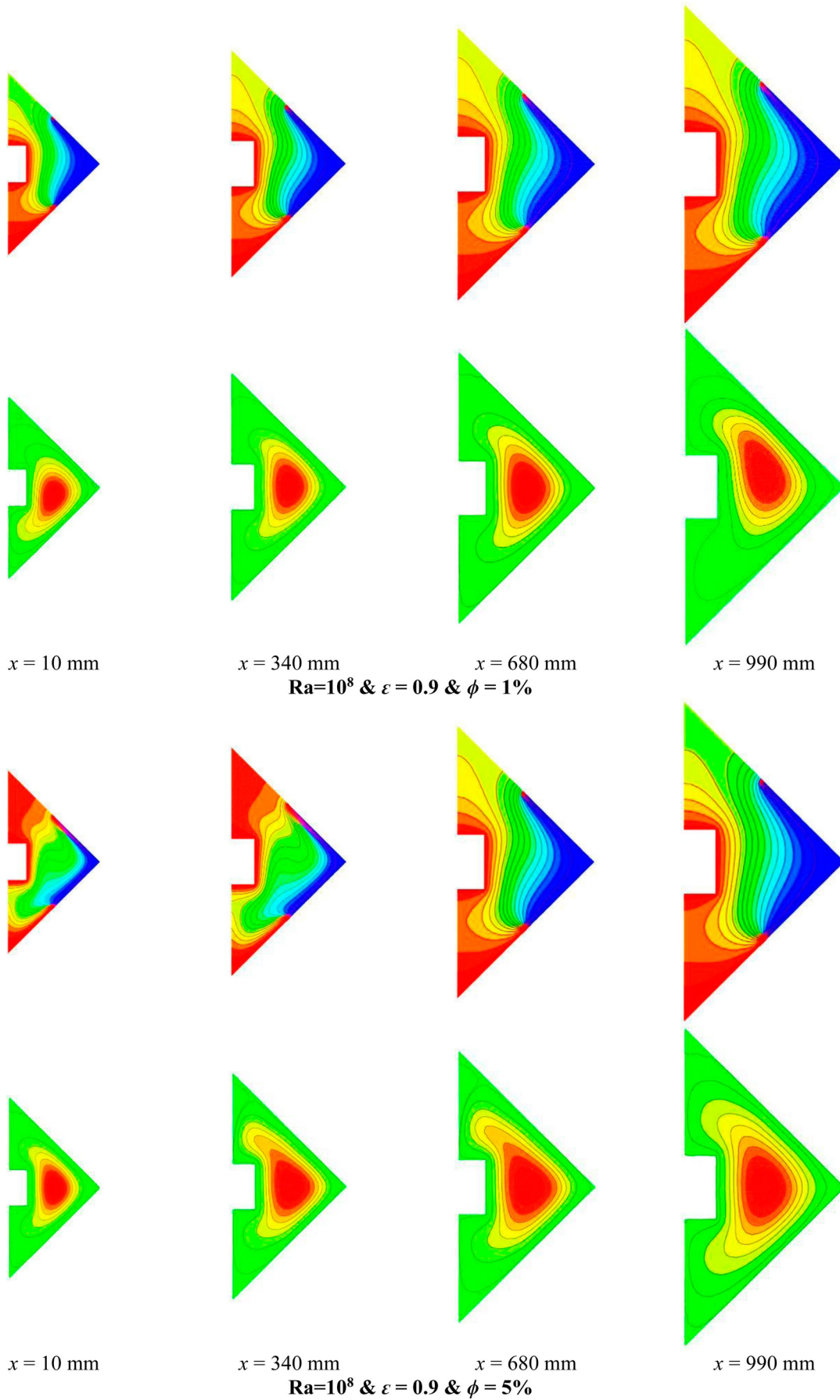


**Figure 14.** Temperature and velocity contours for various nanoparticle volume fractions and at various cross sections of a 3D cavity with  $\varepsilon = 0.9$  and  $Ra = 10^8$  for a case with  $T_h = 400 \text{ K}$  and a heated obstacle.



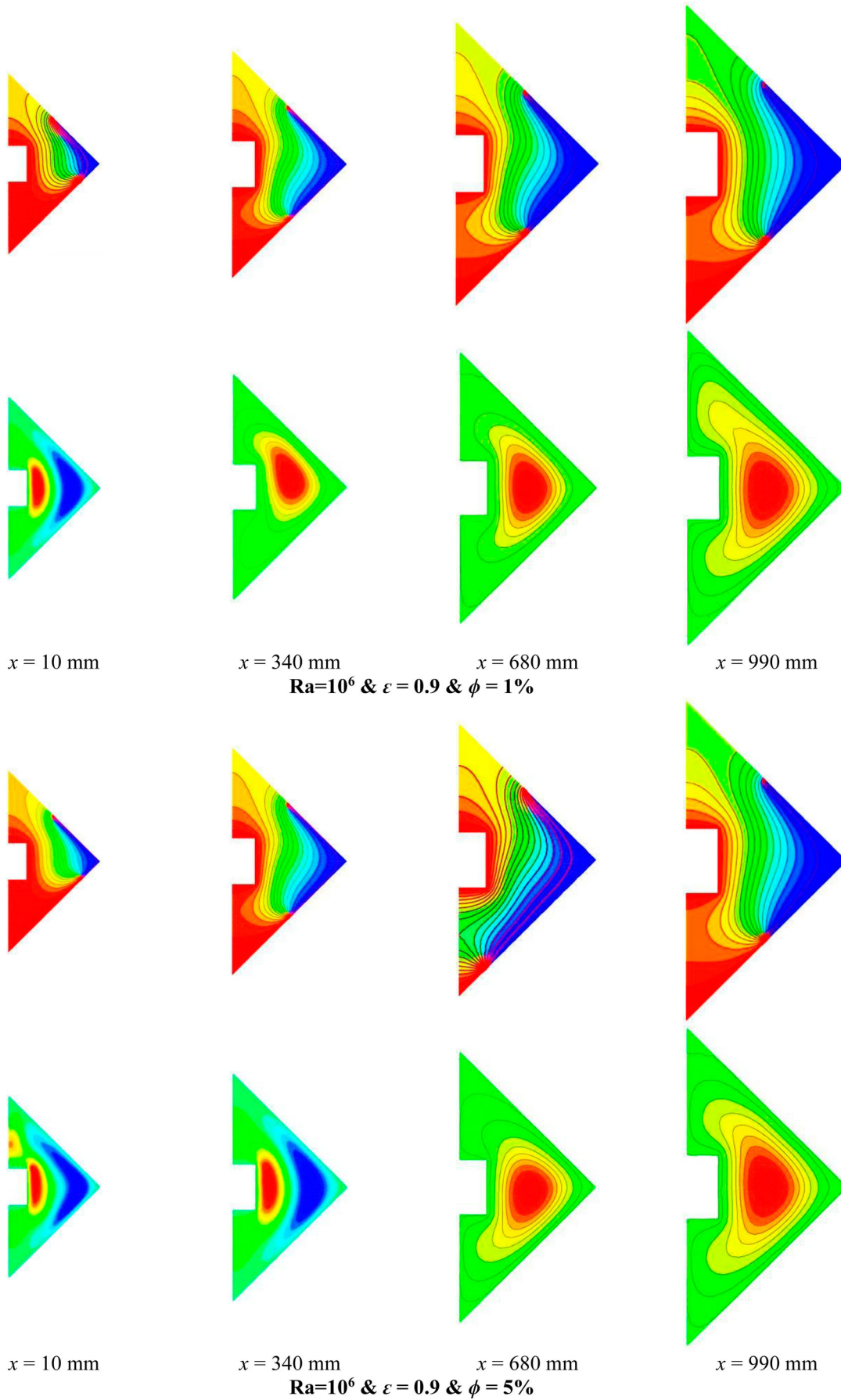


**Figure 15.** Temperature and velocity contours for various nanoparticle volume fractions and at various cross sections of a 3D cavity with  $\varepsilon = 0.9$  and  $Ra = 10^6$  for a case with  $T_h = 500 \text{ K}$  and a heated obstacle.

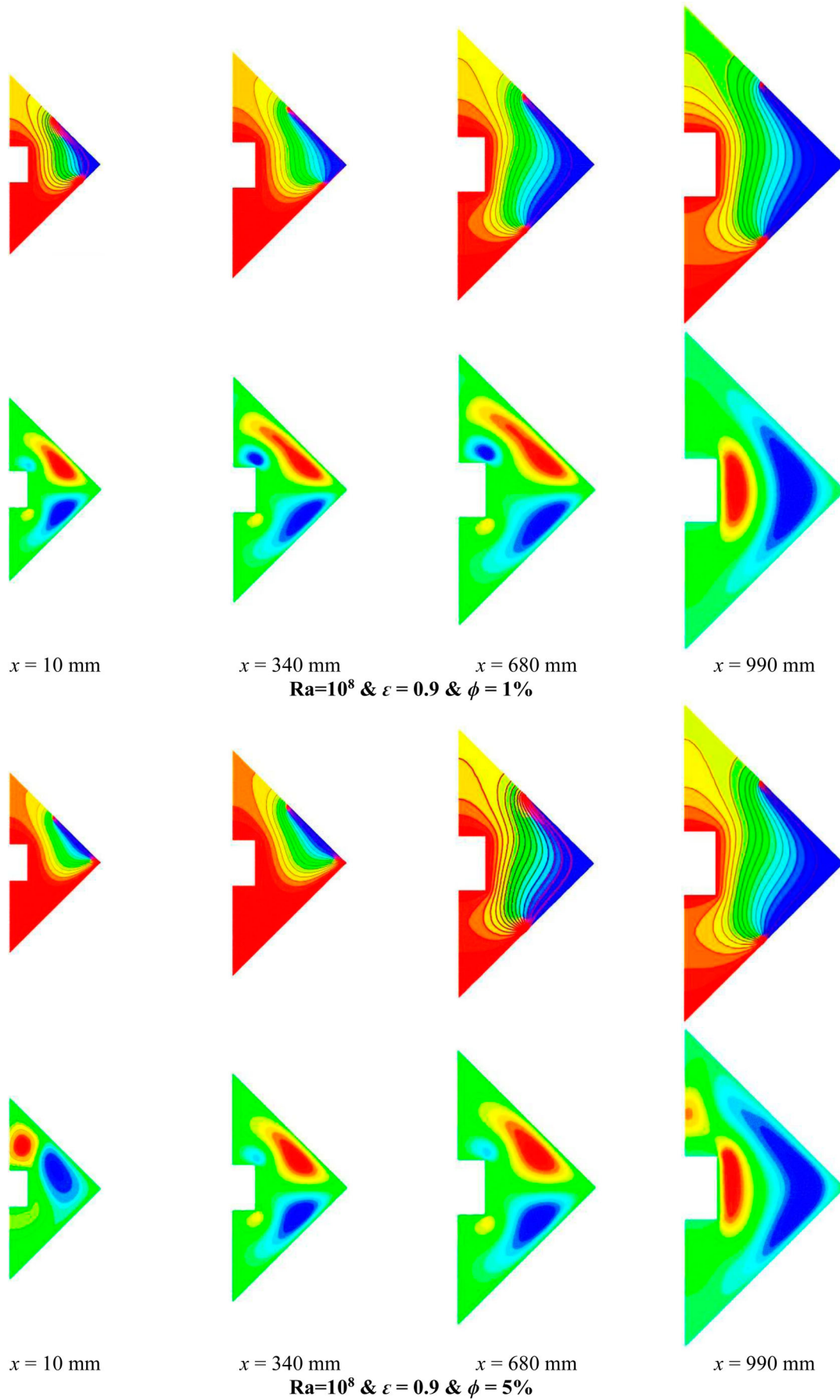


**Figure 16.** Temperature and velocity contours for various nanoparticle volume fractions and at various cross sections of a 3D cavity with  $\varepsilon = 0.9$  and  $\text{Ra} = 10^8$  for a case with  $T_h = 500$  K and a heated obstacle.

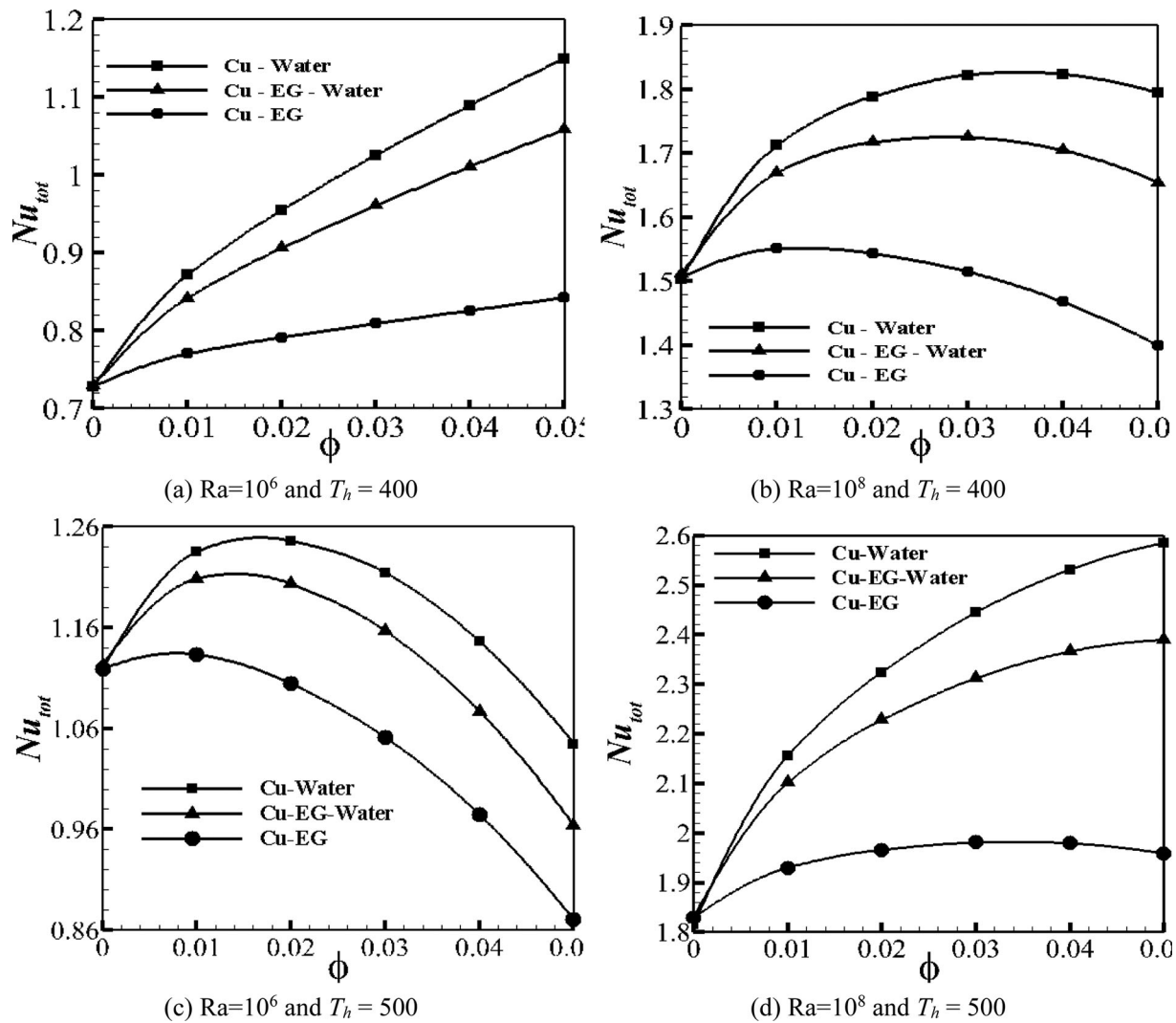


**Figure 17.** Predicted total Nu versus different NF volume fractions for different base fluids for a 3D cavity with  $\varepsilon = 0.3$  and  $Ra = 10^6$  and  $10^8$  for cases with  $T_h = 400$  and  $500$  K and a heated obstacle.

the base fluid, the predicted mean Nu is more than for all other models in all ranges of nanoparticle concentrations studied when the base fluids are ethylene-glycol/water or ethylene-glycol, respectively. As seen in Figure 17(b) for the case with  $Ra = 10^8$  and  $T_h = 400$ , the predicted average Nu is always raised by increasing the volume concentration of nanoparticles  $\phi$  until a nanoparticle volume fraction of 0.01 (for ethylene-glycol), 0.02 (for ethylene-glycol/water) and 0.03 (for water) is reached, and then the Nusselt number values reduce. Consequently, there is an optimum nanoparticle volume fraction/concentration  $\phi$  for each model that leads to the highest Nusselt number.

As shown in Figure 17(c) for the case with  $Ra = 10^6$  and  $T_h = 500$ , the predicted average Nusselt number is always increased by increasing the number of nanoparticles until a nanoparticle volume fraction of 0.02 (for water and ethylene-glycol/water) and 0.01 (for ethylene-glycol) is reached, and then the Nusselt number values

reduce. Consequently, there is an optimum nanoparticle volume fraction  $\phi$  for each model that leads to the highest Nu. As shown in Figure 17(d) for the case with  $Ra = 10^8$  and  $T_h = 500$ , the predicted average Nu is always raised by increasing the number of nanoparticles until a nanoparticle volume fraction of 0.03 (for ethylene-glycol/water) is reached, and then the Nusselt number values reduce. Also, for the ethylene-glycol model and the water cases, the average Nu is always increased by increasing the nanoparticle volume fraction. Consequently, there is an optimum nanoparticle volume fraction  $\phi$  for each model that leads to the highest Nusselt number.

#### 4. Conclusion

The chief objective of the current study was to investigate numerically the effects of the emissivity of the

material, the Rayleigh number, and the volume fraction of nanoparticles (NPs) on the thermal and flow characteristics of a three-dimensional diamond-shaped cavity fitted with a square-shaped barrier having reducing dimensions:

- two-phase NF flow and heat transfer were modeled numerically;
- a 3D diamond-shaped cavity was simulated using symmetric boundary conditions;
- the effects of using a square-shaped obstacle having decreasing dimensions were analyzed;
- copper nanoparticles were added to the base fluid for making the nanofluid;
- the influences of different emissivity values, Rayleigh numbers and nanoparticle volume fractions were investigated.

The important findings of the investigation are summarized as follows.

- On the left-hand sides of cavities, which have smaller dimensions, the rate of HT is stronger. Also, it is seen that, in all cases, a clockwise and also a counter-clockwise vortex exist in the cavities because of temperature gradients.
- Increasing the volume concentration  $\phi$  of NFs in the base fluid results in enhanced heat transfer (HT) without showing any significant change in the streamlines.
- Enhanced HT is also noticed at higher values of Ra.
- In the case of using material with an emissivity of 0.3, usage of the cavity with a heated obstacle and a constant hot-side temperature of 400 or 500 K should be suggested.
- At higher  $\phi$  and Ra, augmentation in HT is reported.
- The emissivity coefficient does not influence the thermal or flow characteristics of nanofluids.
- For the case with  $Ra = 10^6$  and  $T_h = 400$  K, the predicted Nu is always raised by increasing the nanoparticle volume concentration  $\phi$ , and consequently, at a nanoparticle volume fraction of 0.05, the highest Nusselt number is achieved.
- It is realized that, for water as the base fluid, the predicted mean Nu is more than for all other models in all ranges of nanoparticle concentrations studied when the base fluids are ethylene-glycol/water or ethylene-glycol, respectively.
- For the case with  $Ra = 10^8$  and  $T_h = 400$  K, the predicted Nu is always raised by increasing the number of nanoparticles  $\phi$  until a nanoparticle volume fraction of 0.01 (for ethylene-glycol), 0.02 (for

ethylene-glycol/water) and 0.03 (for water) is reached, and then the Nusselt number values reduce.

- There is an optimum nanoparticle volume fraction for each model that leads to the highest Nu.
- For the case with  $Ra = 10^6$  and  $T_h = 500$  K, the predicted average Nusselt number is always increased by increasing the nanoparticle concentration  $\phi$  until a nanoparticle volume fraction of 0.02 (for water and ethylene-glycol/water) and 0.01 (for ethylene-glycol) is reached, and then the Nusselt number values reduce.
- For the case with  $Ra = 10^8$  and  $T_h = 500$  K, the predicted average Nusselt number is always increased by increasing the nanoparticle concentration  $\phi$  until a nanoparticle volume fraction of 0.03 (for ethylene-glycol/water) is reached, and then the Nusselt number values reduce. Also, for the ethylene-glycol model and water case, the average Nusselt number is always increased by increasing the nanoparticle volume fraction.
- This paper offers an appropriate simulation method for the investigation of 3D symmetrical geometries that are filled with two-phase nanofluids, when both radiation and convection equations are solved.

## Nomenclature

$c_p$	Specific heat (J/kg·K)
Cu	Copper
$d_{np}$	Nanoparticle size (nm)
$\vec{g}$	Gravity ( $m/s^2$ )
$k$	Thermal conductivity (W/m·K)
Ra	Rayleigh number (–)
$M$	Molecular weight of the base fluid (kg/kmol)
$N$	Avogadro's number (–)
Nu	Nusselt number (–)
$\vec{P}$	Pressure (Pa)
$T_c$	Cold side temperature (K)
$T_{fr}$	Liquid freezing point of base fluid (K)
$T_h$	Hot-side temperature (K)
$T_{initial}$	Initial nanofluid temperature (K)
$T_m$	Each section-temperature (K)
$\vec{U}_{dr,bf}$	Nanoparticle drift velocity (m/s)
$\vec{U}_{dr,s}$	Fluid drift velocity (m/s)
$u_B$	Average Brownian velocity (m/s)

## Greek symbols

$\vec{\alpha}$	Acceleration ( $m/s^2$ )
$\rho$	Density ( $kg/m^3$ )
$\varepsilon$	Emissivity (–)
$\phi$	volume concentration of nanoparticles (%)
$\mu$	Dynamic viscosity (Pa·s)



## Disclosure statement

No potential conflict of interest was reported by the authors.

## References

- Aghayari, R., Maddah, H., Pourkiaei, S. M., Ahmadi, M. H., Chen, L., & Ghazvini, M. (2020). Theoretical and experimental studies of heat transfer in a double-pipe heat exchanger equipped with twisted tape and nanofluid. *European Physical Journal Plus*, 135(2). <https://doi.org/10.1140/epjp/s13360-020-00252-8>
- Ahmadi, M. H., Ghahremanzhad, A., Chau, K.-W., Seifadini, P., Ramezannezhad, M., & Ghasempour, R. (2019). Development of simple-to-use predictive models to determine thermal properties of Fe<sub>2</sub>O<sub>3</sub>/water-ethylene glycol nanofluid. *Computation*, 7(1), 18. <https://doi.org/10.3390/computation7010018>
- Ahmadi, M. H., Ghazvini, M., Maddah, H., Kahani, M., Pourfarhang, S., Pourfarhang, A., & Heris, S. Z. (2020). Prediction of the pressure drop for CuO/(ethylene glycol-water) nanofluid flows in the car radiator by means of artificial neural networks analysis integrated with genetic algorithm. *Physica A: Statistical Mechanics and Its Applications*, 546, 124008. <https://doi.org/10.1016/j.physa.2019.124008>
- Al-Ansary, H., & Zeitoun, O. (2011). Numerical study of conduction and convection heat losses from a half-insulated air-filled annulus of the receiver of a parabolic trough collector. *Solar Energy*, 85(11), 3036–3045. <https://doi.org/10.1016/j.solener.2011.09.002>
- Aladdin, N. A. L., Bachok, N., & Pop, I. (2020). Cu-Al<sub>2</sub>O<sub>3</sub>/water hybrid nanofluid flow over a permeable moving surface in presence of hydromagnetic and suction effects. *Alexandria Engineering Journal*, 59(2), 657–666. <https://doi.org/10.1016/j.aej.2020.01.028>
- Alsabery, A. I., Gedik, E., Chamkha, A. J., & Hashim, I. (2020). Impacts of heated rotating inner cylinder and two-phase nanofluid model on entropy generation and mixed convection in a square cavity. *Heat and Mass Transfer/Waerme- Und Stoffuebertragung*, 56(1), 321–338. <https://doi.org/10.1007/s00231-019-02698-8>
- Alsabery, A. I., Ismael, M. A., Chamkha, A. J., & Hashim, I. (2020). Effect of nonhomogeneous nanofluid model on transient natural convection in a non-Darcy porous cavity containing an inner solid body. *International Communications in Heat and Mass Transfer*, 110, 104442. <https://doi.org/10.1016/j.icheatmasstransfer.2019.104442>
- Alsabery, A. I., Mohebbi, R., Chamkha, A. J., & Hashim, I. (2019). Impacts of magnetic field and non-homogeneous nanofluid model on convective heat transfer and entropy generation in a cavity with heated trapezoidal body. *Journal of Thermal Analysis and Calorimetry*, 138(2), 1371–1394. <https://doi.org/10.1007/s10973-019-08249-x>
- Alsarraf, J., Moradikazerouni, A., Shahsavari, A., Afrand, M., Salehipour, H., & Tran, M. D. (2019). Hydrothermal analysis of turbulent boehmite alumina nanofluid flow with different nanoparticle shapes in a minichannel heat exchanger using two-phase mixture model. *Physica A: Statistical Mechanics and Its Applications*, 520, 275–288. <https://doi.org/10.1016/j.physa.2019.01.021>
- Arani, A. A. A., Sadripour, S., & Kermani, S. (2017). Nanoparticle shape effects on thermal-hydraulic performance of boehmite alumina nanofluids in a sinusoidal-wavy minichannel with phase shift and variable wavelength. *International Journal of Mechanical Sciences*, 128–129, 550–563. <https://doi.org/10.1016/j.ijmecsci.2017.05.030>
- Ayoubi Ayoubloo, K., Ghalambaz, M., Armaghani, T., Noghrehabadi, A., & Chamkha, A. J. (2019). Pseudoplastic natural convection flow and heat transfer in a cylindrical vertical cavity partially filled with a porous layer. *International Journal of Numerical Methods for Heat and Fluid Flow*, 30(3), 1096–1114. <https://doi.org/10.1108/HFF-06-2019-0464>
- Baghban, A., Sasanipour, J., Pourfayaz, F., Ahmadi, M. H., Kasaean, A., Chamkha, A. J., Oztop, H. F., & Chau, K. W. (2019). Towards experimental and modeling study of heat transfer performance of water- SiO<sub>2</sub> nanofluid in quadrangular cross-section channels. *Engineering Applications of Computational Fluid Mechanics*, 13(1), 453–469. <https://doi.org/10.1080/19942060.2019.1599428>
- Barnoon, P., Toghraie, D., Eslami, F., & Mehmandoust, B. (2019). Entropy generation analysis of different nanofluid flows in the space between two concentric horizontal pipes in the presence of magnetic field: Single-phase and two-phase approaches. *Computers and Mathematics with Applications*, 77(3), 662–692. <https://doi.org/10.1016/j.camwa.2018.10.005>
- Beigzadeh, M., Pourfayaz, F., & Ahmadi, M. H. (2020). Modeling and improvement of solid oxide fuel cell-single effect absorption chiller hybrid system by using nanofluids as heat transporters. *Applied Thermal Engineering*, 166, 114707. <https://doi.org/10.1016/j.applthermaleng.2019.114707>
- Chamkha, A. J., Sazegar, S., Jamesahar, E., & Ghalambaz, M. (2019). Thermal non-equilibrium heat transfer modeling of hybrid nanofluids in a structure composed of the layers of solid and porous media and free nanofluids. *Energies*, 12(3), 541. <https://doi.org/10.3390/en12030541>
- Corcione, M. (2011). Empirical correlating equations for predicting the effective thermal conductivity and dynamic viscosity of nanofluids. *Energy Conversion and Management*, 52(1), 789–793. <https://doi.org/10.1016/j.enconman.2010.06.072>
- Dogonchi, A. S., Tayebi, T., Chamkha, A. J., & Ganji, D. D. (2020). Natural convection analysis in a square enclosure with a wavy circular heater under magnetic field and nanoparticles. *Journal of Thermal Analysis and Calorimetry*, 139(1), 661–671. <https://doi.org/10.1007/s10973-019-08408-0>
- Ez Abadi, A. M., Sadi, M., Farzaneh-Gord, M., Ahmadi, M. H., Kumar, R., & Chau, K. W. (2020). A numerical and experimental study on the energy efficiency of a regenerative heat and mass exchanger utilizing the counter-flow Maisotsenko cycle. *Engineering Applications of Computational Fluid Mechanics*, 14(1), 1–12. <https://doi.org/10.1080/19942060.2019.1617193>
- Fereidoon, A., Saedodin, S., Hemmat Esfe, M., & Noroozi, M. J. (2013). Evaluation of mixed convection in inclined square lid-driven cavity filled with al<sub>2</sub>o<sub>3</sub>/water nano-fluid. *Engineering Applications of Computational Fluid Mechanics*, 7(1), 55–65. <https://doi.org/10.1080/19942060.2013.11015453>
- Gan, T., Ming, T., Fang, W., Liu, Y., Miao, L., Ren, K., & Ahmadi, M. H. (2020). Heat transfer enhancement of a microchannel heat sink with the combination of impinging jets, dimples, and side outlets. *Journal of Thermal Analysis and Calorimetry*, 141(1), 45–56. <https://doi.org/10.1007/s10973-019-08754-z>

- Ghahremanezhad, A., Xu, H., Alhuyi Nazari, M., Hossein Ahmadi, M., & Vafai, K. (2019). Effect of porous substrates on thermohydraulic performance enhancement of double layer microchannel heat sinks. *International Journal of Heat and Mass Transfer*, 131, 52–63. <https://doi.org/10.1016/j.ijheatmasstransfer.2018.11.040>
- Ghalandari, M., Mirzadeh Koooshahi, E., Mohamadian, F., Shamshirband, S., & Chau, K. W. (2019). Numerical simulation of nanofluid flow inside a root canal. *Engineering Applications of Computational Fluid Mechanics*, 13(1), 254–264. <https://doi.org/10.1080/19942060.2019.1578696>
- Giwa, S. O., Sharifpur, M., & Meyer, J. P. (2020). Experimental study of thermo-convection performance of hybrid nanofluids of Al<sub>2</sub>O<sub>3</sub>-MWCNT/water in a differentially heated square cavity. *International Journal of Heat and Mass Transfer*, 148, 119072. <https://doi.org/10.1016/j.ijheatmasstransfer.2019.119072>
- He, W., Toghraie, D., Lotfipour, A., Pourfattah, F., Karimipour, A., & Afrand, M. (2020). Effect of twisted-tape inserts and nanofluid on flow field and heat transfer characteristics in a tube. *International Communications in Heat and Mass Transfer*, 110(December 2019), 104440. <https://doi.org/10.1016/j.icheatmasstransfer.2019.104440>
- Heris, S. Z., Kazemi-Beydokhti, A., Noie, S. H., & Rezvan, S. (2012). Numerical study on convective heat transfer of Al<sub>2</sub>O<sub>3</sub>/water, CuO/water and Cu/water nanofluids through square cross-section duct in laminar flow. *Engineering Applications of Computational Fluid Mechanics*, 6(1), 1–14. <https://doi.org/10.1080/19942060.2012.11015398>
- Hoseinzadeh, S., Moafi, A., Shirkhani, A., & Chamkha, A. J. (2019). Numerical validation heat transfer of rectangular cross-section porous fins. *Journal of Thermophysics and Heat Transfer*, 33(3), 698–704. <https://doi.org/10.2514/1.T5583>
- Jilte, R., Ahmadi, M. H., Kumar, R., Kalamkar, V., & Mosavi, A. (2020). Cooling performance of a novel circulatory flow concentric multi-channel heat sink with nanofluids. *Nanomaterials*, 10(4), 647. <https://doi.org/10.3390/nano10040647>
- Karami, M., Farahani, S. D., Kowsary, F., & Mosavi, A. (2020). Experimental estimation of temporal and spatial resolution of coefficient of heat transfer in a channel using inverse heat transfer method. *Engineering Applications of Computational Fluid Mechanics*, 14(1), 271–283. <https://doi.org/10.1080/19942060.2020.1712261>
- Karimi, A., Al-Rashed, A. A. A., Afrand, M., Mahian, O., Wongwises, S., & Shahsavari, A. (2019). The effects of tape insert material on the flow and heat transfer in a nanofluid-based double tube heat exchanger: Two-phase mixture model. *International Journal of Mechanical Sciences*, 156(April), 397–409. <https://doi.org/10.1016/j.ijmecsci.2019.04.009>
- Khodabandeh, E., Boushehri, R., Akbari, O. A., Akbari, S., & Toghraie, D. (2020). Numerical investigation of heat and mass transfer of water—Silver nanofluid in a spiral heat exchanger using a two-phase mixture method. *Journal of Thermal Analysis and Calorimetry*, 144, 1003–1012. <https://doi.org/10.1007/s10973-020-09533-x>
- Kim, D., Kwon, Y., Cho, Y., Li, C., Cheong, S., Hwang, Y., Lee, J., Hong, D., & Moon, S. (2009). Convective heat transfer characteristics of nanofluids under laminar and turbulent flow conditions. *Current Applied Physics*, 9(2 Suppl), e119–e123. <https://doi.org/10.1016/j.cap.2008.12.047>
- Leong, W. H., Hollands, K. G. T., & Brunger, A. P. (1998). Experimental Nusselt numbers for a cubical-cavity benchmark problem in natural convection. *International Journal of Heat and Mass Transfer*, 42(11), 1979–1989. [https://doi.org/10.1016/S0017-9310\(98\)00299-3](https://doi.org/10.1016/S0017-9310(98)00299-3)
- Maddah, H., Ghazvini, M., & Ahmadi, M. H. (2019). Predicting the efficiency of CuO/water nanofluid in heat pipe heat exchanger using neural network. *International Communications in Heat and Mass Transfer*, 104(March), 33–40. <https://doi.org/10.1016/j.icheatmasstransfer.2019.02.002>
- Mahdavi, M., Sharifpur, M., & Meyer, J. P. (2017). A novel combined model of discrete and mixture phases for nanoparticles in convective turbulent flow. *Physics of Fluids*, 29(8), 082005. <https://doi.org/10.1063/1.4998181>
- Mashayekhi, R., Khodabandeh, E., Bahiraei, M., Bahrami, L., Toghraie, D., & Akbari, O. A. (2017). Application of a novel conical strip insert to improve the efficacy of water–Ag nanofluid for utilization in thermal systems: A two-phase simulation. *Energy Conversion and Management*, 151, 573–586. <https://doi.org/10.1016/j.enconman.2017.09.025>
- Mehryan, S. A. M., Izadi, M., Namazian, Z., & Chamkha, A. J. (2019). Natural convection of multi-walled carbon nanotube–Fe<sub>3</sub>O<sub>4</sub>/water magnetic hybrid nanofluid flowing in porous medium considering the impacts of magnetic field-dependent viscosity. *Journal of Thermal Analysis and Calorimetry*, 138(2), 1541–1555. <https://doi.org/10.1007/ss10973-019-08164-1>
- Mehryan, S. A. M., Izadpanahi, E., Ghalambaz, M., & Chamkha, A. J. (2019). Mixed convection flow caused by an oscillating cylinder in a square cavity filled with Cu–Al<sub>2</sub>O<sub>3</sub>/water hybrid nanofluid. *Journal of Thermal Analysis and Calorimetry*, 137(3), 965–982. <https://doi.org/10.1007/s10973-019-08012-2>
- Milani Shirvan, K., Mamourian, M., Mirzakhani, S., & Ellahi, R. (2017). Numerical investigation of heat exchanger effectiveness in a double pipe heat exchanger filled with nanofluid: A sensitivity analysis by response surface methodology. *Powder Technology*, 313, 99–111. <https://doi.org/10.1016/j.powtec.2017.02.065>
- Neystani, M., Nazari, M., Shahmardan, M. M., Sharifpur, M., Ashouri, M., & Meyer, J. P. (2019). Thermal characteristics of CPU cooling by using a novel porous heat sink and nanofluids: Comparative experimental study. *Journal of Thermal Analysis and Calorimetry*, 138(1), 805–817. <https://doi.org/10.1007/s10973-019-08256-y>
- Patankar, S. V. (1980). *Numerical heat transfer and fluid flow*. <https://doi.org/10.13182/nse81-a20112>
- Ramezanizadeh, M., Alhuyi Nazari, M., Ahmadi, M. H., & Chau, K. W. (2019). Experimental and numerical analysis of a nanofluidic thermosyphon heat exchanger. *Engineering Applications of Computational Fluid Mechanics*, 13(1), 40–47. <https://doi.org/10.1080/19942060.2018.1518272>
- Sadrupour, S. (2019). 3D numerical analysis of atmospheric-aerosol/carbon-black nanofluid flow within a solar air heater located in Shiraz, Iran. *International Journal of Numerical Methods for Heat and Fluid Flow*, 29(4), 1378–1402. <https://doi.org/10.1108/HFF-04-2018-0169>
- Sadrupour, S., & Chamkha, A. J. (2019). The effect of nanoparticle morphology on heat transfer and entropy generation of supported nanofluids in a heat sink solar collector. *Thermal Science and Engineering Progress*, 9, 266–280. <https://doi.org/10.1016/j.tsep.2018.12.002>

- Salari, A., Kazemian, A., Ma, T., Hakkaki-Fard, A., & Peng, J. (2020). Nanofluid based photovoltaic thermal systems integrated with phase change materials: Numerical simulation and thermodynamic analysis. *Energy Conversion and Management*, 205, 112384. <https://doi.org/10.1016/j.enconman.2019.112384>
- Samadifar, M., & Toghraie, D. (2018). Numerical simulation of heat transfer enhancement in a plate-fin heat exchanger using a new type of vortex generators. *Applied Thermal Engineering*, 133, 671–681. <https://doi.org/10.1016/j.applthermaleng.2018.01.062>
- Selimefendigil, F., Öztop, H. F., & Chamkha, A. J. (2019). Mixed convection of pulsating ferrofluid flow over a backward-facing step. *Iranian Journal of Science and Technology, Transactions of Mechanical Engineering*, 43(4), 593–612. <https://doi.org/10.1007/s40997-018-0238-x>
- Sharifpur, M., Solomon, A. B., Ottermann, T. L., & Meyer, J. P. (2018). Optimum concentration of nanofluids for heat transfer enhancement under cavity flow natural convection with TiO<sub>2</sub> – Water. *International Communications in Heat and Mass Transfer*, 98(October), 297–303. <https://doi.org/10.1016/j.icheatmasstransfer.2018.09.010>
- Sharma, J. P., Sharma, A., Jilte, R. D., Kumar, R., & Ahmadi, M. H. (2020). A study on thermohydraulic characteristics of fluid flow through microchannels. *Journal of Thermal Analysis and Calorimetry*, 140(1), 1–32. <https://doi.org/10.1007/s10973-019-08741-4>
- Shashikumar, N., Gireesha, B. J., Mahanthesh, B., Prasannakumara, B., & Chamkha, A. J. (2019). Entropy generation analysis of magneto-nanofluids embedded with aluminium and titanium alloy nanoparticles in microchannel with partial slips and convective conditions. *International Journal of Numerical Methods for Heat and Fluid Flow*, 29(10), 3638–3658. <https://doi.org/10.1108/HFF-06-2018-0301>
- Sheikholeslami, M., Jafaryar, M., Abohamzeh, E., Shafee, A., & Babazadeh, H. (2020). Energy and entropy evaluation and two-phase simulation of nanoparticles within a solar unit with impose of new turbulator. *Sustainable Energy Technologies and Assessments*, 39, 100727. <https://doi.org/10.1016/j.seta.2020.100727>
- Siavashi, M., Bahrami, H. R. T., & Saffari, H. (2017). Numerical investigation of porous rib arrangement on heat transfer and entropy generation of nanofluid flow in an annulus using a two-phase mixture model. *Numerical Heat Transfer, Part A: Applications*, 71(12), 1251–1273. <https://doi.org/10.1080/10407782.2017.1345270>
- Tayebi, T., Chamkha, A. J., & Djezzar, M. (2019). Natural convection of CNT-water nanofluid in an annular space between confocal elliptic cylinders with constant heat flux on inner wall. *Scientia Iranica*, 26(5 B), 0–0. <https://doi.org/10.24200/sci.2018.21069>
- Varzaneh, A. A., Toghraie, D., & Karimipour, A. (2020). Comprehensive simulation of nanofluid flow and heat transfer in straight ribbed microtube using single-phase and two-phase models for choosing the best conditions. *Journal of Thermal Analysis and Calorimetry*, 139(1), 701–720. <https://doi.org/10.1007/s10973-019-08381-8>
- Vatani, A., & Mohammed, H. A. (2013). Turbulent nanofluid flow over periodic rib-grooved channels. *Engineering Applications of Computational Fluid Mechanics*, 7(3), 369–381. <https://doi.org/10.1080/19942060.2013.11015478>
- Xu, Y., Islam, M. D., & Kharoua, N. (2017). Numerical study of winglets vortex generator effects on thermal performance in a circular pipe. *International Journal of Thermal Sciences*, 112. <https://doi.org/10.1016/j.ijthermalsci.2016.10.015>